



Multi-proxy record of the mid-Maastrichtian event in the European Chalk Sea: Paleoceanographic implications



Zofia Dubicka^{a,b,*}, Weronika Wierny^{a,c}, Maciej J. Bojanowski^d, Michał Rakociński^e, Ireneusz Walaszczyk^a, Nicolas Thibault^f

^a Faculty of Geology, University of Warsaw, Warsaw 02-089, Poland

^b GFZ German Research Centre for Geosciences, Telegrafenberg, 14473 Potsdam, Germany

^c Polish Geological Institute-National Research Institute, Rakowiecka 4, 00-975 Warszawa, Poland

^d Institute of Geological Sciences, Polish Academy of Sciences, Warsaw, Poland

^e Faculty of Natural Sciences, University of Silesia in Katowice, Będzińska 60, 41-200 Sosnowiec, Poland

^f Department of Geosciences and Natural Resource Management, University of Copenhagen, 1350 Copenhagen K, Denmark

ARTICLE INFO

Article history:

Received 11 September 2023

Revised 26 November 2023

Accepted 27 November 2023

Available online 30 November 2023

Handling editor: Ian David Somerville

Keywords:

Extinction

Large Igneous Province (LIP)

Sea-level

Climate warming

Cretaceous

ABSTRACT

The Cretaceous provides us with an excellent case history of ocean-climate-biota system perturbations. Such perturbations occurred several times during the Cretaceous, such as oceanic anoxic events and the end-Cretaceous mass extinction, which have been the subject of an abundant literature. Other perturbations, such as the mid-Maastrichtian Event (MME) remain poorly understood. The MME was associated with global sea-level rise, changes in climate and deep-water circulation that were accompanied by biotic extinctions including 'true inoceramids' and the demise of the Caribbean-Tethyan rudist reef ecosystems. So far, the context and causes behind the MME remain poorly studied. We conducted high-resolution integrated biotic, petrological and geochemical studies in order to fill this knowledge gap. We studied, in particular, carbonate Nd and Os isotopes, whole-rock Hg, C and N content, C and N isotopes in organic matter, S isotopes in carbonate-associated sulfate, along with C and O isotopes in foraminifera from the European Chalk Sea: the Polanówka UW-1 core from Poland and the Stevns-1 core from Denmark. Our data showed that sea-level rise of ~50–100 m lasted around ~2 Ma and co-occurred with anomalously high mercury concentration in seawater. Along with previously published data, our results strongly suggest that the MME was driven by intense volcanic-tectonic activity, likely related to the production of vast oceanic plateaus (LIP, Large Igneous Province). The collapse of reef ecosystems could have been the consequence of LIP-related environmental stress factors, including climate warming, presumably caused by emission of greenhouse gases, modification of the oceanic circulation, oceanic acidification and/or toxic metal input. The disappearance of the foraminifer *Stensioeina* lineage on the European shelf was likely caused by the collapse of primary production triggered by sea-level rise and limited amount of nutrient input. Nd isotopes and foraminiferal assemblages attest for changes in sea-water circulation in the European Shelf and the increasing contribution of North Atlantic water masses.

© 2023 The Authors. Published by Elsevier B.V. on behalf of International Association for Gondwana Research. This is an open access article under the CC BY license (<http://creativecommons.org/licenses/by/4.0/>).

1. Introduction

The Late Cretaceous was a period of Earth's history characterised by high sea-levels, large epicontinental seas, reduced land and high temperatures across the globe – a 'Greenhouse world', with a much higher concentration of atmospheric CO₂ than today. Deep ocean and land surface temperatures were ca. 10 °C higher

than today (Skelton, 2003). After a peak in greenhouse conditions with maximum sea surface temperature recorded in the mid-Cretaceous (Albian-Turonian), a long-term Late Cretaceous cooling trend reached a climax in the latest Campanian and Maastrichtian (e.g., Huber et al., 2002). Superimposed on this long-term trend, worldwide documentation of several episodes of climatic cooling and warming correlated with eustatic sea-level changes indicate climate instability and increased ocean dynamics in the Maastrichtian (e.g., Barrera and Savin, 1999; Isaza-Londoño et al., 2006). Some authors speculated that these sea-level fluctuations were controlled by the development of moderate-sized ice sheets

* Corresponding author

E-mail addresses: z.dubicka@uw.edu.pl (Z. Dubicka), weronika.wierny@pgi.gov.pl (W. Wierny).

in Antarctica during at least the early Maastrichtian (Miller et al., 1999) while others evoked the aquifer-eustasy mechanism (Sames et al., 2020). Other potential causes might be related with tectonic processes, that shape ocean basin geometry and change the volume of oceanic basins (Jung et al., 2013), possibly associated with the tectonic phase associated with the opening of the South Atlantic (Frank and Arthur, 1999; Friedrich et al., 2009).

The Cretaceous Greenhouse world was colonized by diverse biota (Skelton, 2003) inhabiting the land mosaic, widespread shallow epicontinental seas and ocean, forming an interesting combination of familiar, modern-looking extant groups, such as flowering plants or calcifying marine plankton together with exotic-looking extinct groups – dinosaurs, marine reptiles and cephalopod ammonites and belemnites – most of which were to be lost in the end-Cretaceous mass extinction. However, the Cretaceous-Paleogene (K-Pg) mass extinction was not the only severe biotic crisis that affected Late Cretaceous ecosystems. Just a few million years prior to the K-Pg boundary event, in the middle part of the Maastrichtian, the global rudist reefs, which were important marine ecosystems covering vast areas of tropical seas (Johnson and Kauffman, 1990; Johnson et al., 1996), suffered a demise along with several abundant groups of marine organisms, including ‘true inoceramids’ (MacLeod, 1994; Chauris et al., 1998; MacLeod and Huber, 2001; Gómez-Alday et al., 2004), gastropods (Johnson and Kauffman, 1990) and foraminifera (Dubicka and Peryt, 2012a, b). Although the last rudists were described as having been extinct during the K-Pg transition (*Gyropleura*; Heinberg, 1979), the global collapse of rudist reef ecosystems correlates, in fact, with the base or with the lower part of the *Abathomphalus mayaroensis* foraminiferal Zone of the middle Maastrichtian (Kauffman and Johnson, 1988). Since reef ecosystems and shallow-marine tropical organisms are particularly sensitive to global stress, most of the mass extinctions led to the devastation of such ecosystems and produced intervals known as “reef gaps” (e.g., Copper, 1994; Veron and Hopley, 2011; Racki 2020a).

Along with these biotic changes, the middle Maastrichtian underwent several prominent oceanographic perturbations. Significant global sea-level rise (Hancock, 1975; Hancock, 1993) accompanied by climate and global deep-water circulation changes (Frank and Arthur, 1999; Li and Keller, 1999; Frank et al., 2005; Voigt et al., 2013; Jung et al., 2013) were marked by shifts in $\delta^{13}\text{C}$, $\delta^{18}\text{O}$ and $\epsilon_{\text{Nd}}(t)$ (Frank and Arthur, 1999; Jung et al., 2013). It is hard to understand why the aforementioned paleoenvironmental changes, which are associated with a much smaller amplitude of isotopic excursions than those that took place across the Campanian-Maastrichtian boundary (CMB) interval (c. 7 °C cooling; Linnert et al., 2014; Thibault et al., 2016), actually appear to have had such an important impact on the biota. Comprehensive analysis of the mechanisms of global environmental changes across this episode, coined as the Mid-Maastrichtian Event (MME), has been, however, hindered by (1) the lack of geological sections unaffected by diagenetic alteration and presenting a complete and continuous record of this event, (2) insufficient resolution of sampling, and (3) the lack of application of more advanced geochemical methods. To date, there is only a handful of papers presenting geochemical data encompassing the MME with a sufficient resolution, including stable C and O, Sr and Nd isotopes (Barrera, 1994; Gómez-Alday et al., 2008; Voigt et al., 2013; Jung et al., 2013) and what truly happened during the MME remains largely unknown.

Here, we present an original new dataset of integrated biotic (foraminiferal) and geochemical proxies from the European Shelf Basin, applied to exceptionally well-preserved material from a recently drilled well in Poland (Polanówka UW-1) and from the Stevns-1 well in Denmark (Fig. 1). We integrate micropaleontological studies with a wide range of geochemical data delivered from

the same set of samples such as e.g., carbonate Nd and Os isotopes, whole-rock Hg, C and N content, C and N isotopes in organic matter, S isotopes in carbonate-associated sulfate, along with C and O isotopes in selected benthic and planktonic foraminiferal tests. This work represents, thus far, the first comprehensive study across the MME. Below, we outline the current perspective on paleoceanographic changes across the event and then we show how these new data fill gaps, modify, and detail this knowledge. What emerges is a much clearer picture of the potential causes and complex, interrelated mechanisms that led to this biotic crisis in the European Chalk Sea.

2. Defining the MME

The Mid-Maastrichtian Event (MME) was originally introduced by Kauffman and Johnson (1988) to describe the biotic extinction of the inoceramids and the loss of Caribbean-Tethyan rudist reef ecosystems. Other authors illustrated the MME as an isotopic event expressed by a long-term positive carbon isotope excursion with a superimposed short-term negative shift in its middle part, and associated with a major reorganization of oceanic circulation patterns (Voigt et al., 2012; Vancoppenolle et al., 2022). Thus far, the MME appears as a complex global ocean–climate perturbation that occurred during the mid-Maastrichtian and led to a significant loss of marine biotic diversity.

2.1. Extinction of inoceramid bivalves

The inoceramids were a clade of eurytopic marine bivalves with a continuous Jurassic-Cretaceous record. While they are first reported in the Permian (Kauffman and Runnegar, 1975), these specimens are poorly documented, and inoceramids are completely absent from the Triassic record; as such, this putative first appearance has remained controversial. The Jurassic inoceramids mostly belong to the family Retroceramidae. The first appearance of the family Inoceramidae, which embraces most of the Cretaceous taxa, occurs in the latest Jurassic and earliest Cretaceous (Crampton, 1988; Harries and Crampton, 1998).

The great taxonomic and morphological diversification of the Inoceramidae began in the late Albian (mid-Cretaceous), continuing throughout the Late Cretaceous (e.g., Pergament, 1967; Kauffman, 1975; Kauffman et al., 1994). The group dominated most marine benthic faunas in both low and high latitudes, with numerous taxa recorded globally. The most characteristic evolutionary features of the clade, at least during the Late Cretaceous, is rapid species-level evolution, extensive morphological diversification, and high abundance, with commonly observed stratigraphic flood occurrences. However, published diversity maxima (Pergament, 1967; Tröger, 1976; Voigt, 1995) are derived from highly dynamic systems resulting from the interplay of elevated evolutionary tempos, extinction events, and biogeographic diversification.

Before their final late Maastrichtian extinction, the group experienced a strong decline across the Campanian/Maastrichtian boundary, to the extent that it was almost completely annihilated. However, inoceramids rapidly recovered from this event and entered a new diversification pulse, reaching a maximum in the late early Maastrichtian. The ubiquitous character of this diversity maximum has been widely noted in the Euramerican, Tethyan, and East African biochores (e.g., Tröger and Röhlich, 1991; MacLeod, 1994; Morris, 1995; Walaszczyk et al., 2009; Walaszczyk et al., 2010; Walaszczyk and Kennedy, 2011) and also coincides with an abundance maximum as suggested by the observation of a peak increase in the amount of recorded inoceramid prisms in numerous deep-sea sites of the Tethys, Atlantic, Pacific and Indian oceans

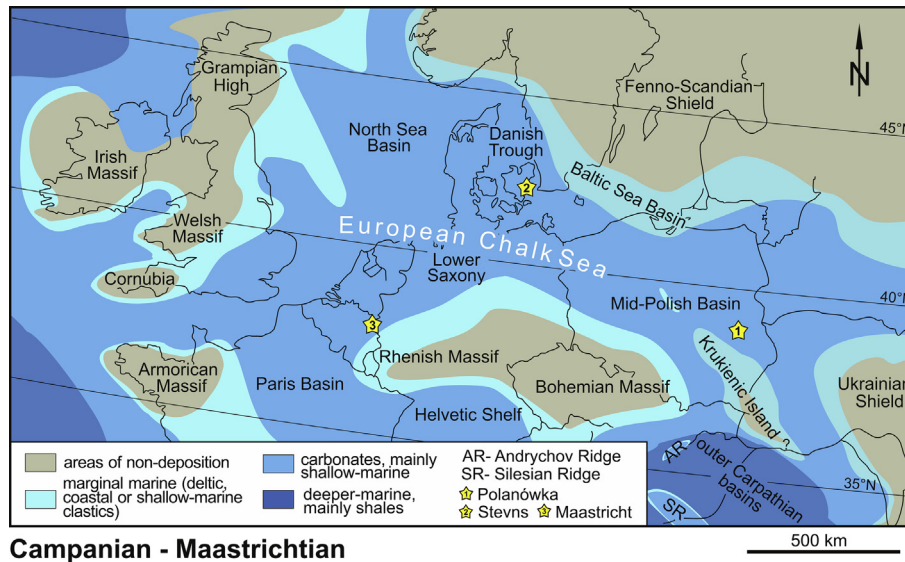


Fig. 1. Paleogeographic map of Western and Central Europe during the Campanian–Maastrichtian (compiled from Ziegler, 1990; Philip et al., 2000) with the Maastrichtian successions discussed in the text.

(MacLeod et al., 1996). Following this diversity and abundance maximum, Inoceramids experienced a critical, final collapse in the late Maastrichtian, well before the K–Pg boundary. This event, placed in the early *Belemnitella junior* belemnite Zone and the early *Abathomphalus mayaroensis* foraminiferal Zone – approximately 2.5 Myr before the end of the Cretaceous (e.g., MacLeod and Ward, 1990; MacLeod and Huber, 1996; Chauris et al., 1998; Gómez-Alday et al., 2004; Nifuku et al., 2009) – aligns well with the timing of the MME. This event is commonly referred to as the extinction of the ‘true inoceramids’, a term used informally for all representatives of the Inoceramidae with the exception of the so-called tegulated inoceramids, of which the genus *Tenuipteria* continued on until the end of the Maastrichtian (e.g., Jagt and Jagt-Yazykova, 2018). Although *Tenuipteria* was once regarded as belonging to Bakevellidae (Cox and Moore, 1969), at the present time there appears to be no good reason to exclude this genus from the family Inoceramidae (Speden, 1970). So far, it remains unclear as to why *Tenuipteria* survived the mid-Maastrichtian ‘true inoceramid’ extinction pulse.

There is no commonly accepted hypothesis that satisfactorily explains the mechanism(s) behind the mid-Maastrichtian Inoceramidae extinction. While it has been suggested that the event is related to habitat limitations, gradual cooling, and/or changing oceanic circulation patterns (Stanley, 1987; Fischer and Bottjer, 1995; MacLeod and Huber, 1996), these drivers were likely insufficient to completely drive the extinction of such a successful eurytopic group. Beyond that, this decline appears to have affected a very successful clade, which only recently had experienced global-scale diversification and dispersion.

2.2. Demise of rudist reef ecosystems

Rudistid bivalves arose in the Late Jurassic (mid-Oxfordian) and became extinct at the end of the Cretaceous, surviving nearly 100 million years (Jones and Nicol, 1986; Skelton, 2003). In the Aptian–Albian, rudists became the main Cretaceous reef builders replacing reef communities previously dominated by corals, algae, sponges, hydrozoans, and bryozoans in the central area of the Tethys (Kauffman and Johnson, 1988; Johnson and Kauffman, 1990). Late Cretaceous rudists had morphologically complex shells, commonly exhibited gigantism, and likely had a rapid growth rate

similarly to modern hermatypic corals (Jones and Nicol, 1986). Cretaceous rudists together with inoceramids comprise species that were among the largest bivalves that ever lived (Nicol, 1964). Although one study suggests that some rare rudist species extended up to the K–Pg boundary (*Gyropleura*; Heinberg, 1979), it has been considered that a global collapse of rudist reef ecosystems occurred during the mid-Maastrichtian, at the base or within the lower part of the *Abathomphalus mayaroensis* foraminiferal Zone (Kauffman and Johnson, 1988). Besides well-documented extinctions of rudists in the Caribbean Province, similar extinctions were documented in sections around the Mediterranean Region (Swinburne, 1991; Kauffman and Hart, 1996), that confirm the global scale of this biotic turnover. The causes for this Cretaceous reef collapse remain poorly understood. Some studies suggested sea level drop and cooling as main causes, responsible for shrinking and eventually disappearance of their habitats (e.g., Johnson, 2002), however, such causes contrast with the global warming and sea-level rise that are characteristic of the mid-Maastrichtian interval.

2.3. Small-amplitude C isotope excursions

Besides the biotic definition of the Mid-Maastrichtian Event (MME) characterised by the aforementioned extinctions of rudist reefs and ‘true inoceramids’, the event has also been defined by (Voigt et al., 2012) as a characteristic plateau of high $\delta^{13}\text{C}$ values that lasted ca. 570 kyr and comprised a suite of 3 delineated carbon isotope excursions (CIEs) MME1 to MME3 (Fig. 2). The lowermost (MME1) and uppermost (MME3) represent positive excursions separated by the MME2 negative shift. These isotope excursions are restrained at Gubbio to the lower half of the C31n magnetostratigraphic unit (Voigt et al., 2010; Voigt et al., 2012; Thibault et al., 2016; Vancoppenolle et al., 2022) and have been well-documented in other locations such as Stevns-1 (Denmark), the Lägerdorf-Kronsmoor-Hemmoor composite section (northern Germany), in the Maastrichtian type area (Netherlands), and in the central Pacific Ocean (Hole 1210B). It must however be noted that at Gubbio, MME2 shows a much higher amplitude than observed at any other locations. The overall MME CIEs have also been identified in continental deposits (Salazar-Jaramillo et al., 2016). Only vague and very general interpretations of these MME $\delta^{13}\text{C}$ excursions

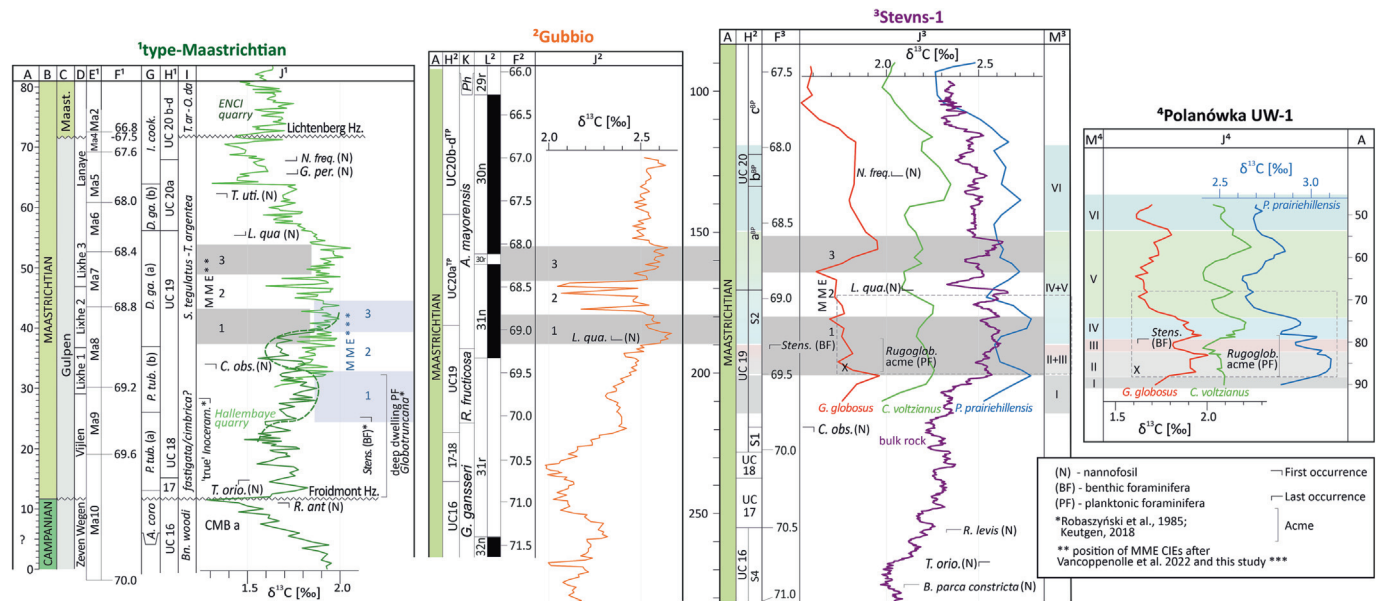


Fig. 2. Bulk $\delta^{13}\text{C}$ (‰ VPDB) curves in the type-Maastrichtian area (Hallembaye and former ENCI quarries), Gubbio and Stevens-1 and foraminifera $\delta^{13}\text{C}$ (‰ VPDB) curves in the Polanówka UW-1 and Stevens-1 boreholes. References: 1 – Vancoppenolle et al., 2022; Keutgen, 2018; Robaszynski et al., 1985; 2 – Vancoppenolle et al., 2022; Voigt et al., 2012; 3 – Surlyk et al., 2013; Voigt et al., 2012; Thibault et al., 2012; this paper. A – depth in meters; B – chronostratigraphy; C, D – lithostratigraphy (C – formations; D – members); E – 405 kyr cycles; F – absolute numerical ages [Ma]; G – dinoflagellate zonation; H – nannofossil zonation; I – macrofossil zonation; J – $\delta^{13}\text{C}$ [‰ V-PDB] curves; K – planktonic foraminiferal zonation; L – magnetostratigraphy; M – geochemical intervals.

have been proposed and refer to disruption of the carbon cycle as a response to a prominent global change in oceanic circulation across the early-late Maastrichtian transition (Voigt et al., 2010; Jung et al., 2013).

2.4. Tectonic forcings on deep-water circulation?

The importance of changes in global oceanic intermediate and deep-water circulation during the MME (Jung et al., 2013) has long been postulated from observations of worldwide $\delta^{18}\text{O}$ and $\delta^{13}\text{C}$ values in benthic foraminifera (Barrera, 1994; Barrera et al., 1997; Frank and Arthur, 1999; Barrera and Savin, 1999; Friedrich et al., 2009) together with more recent studies on the Nd isotopic composition of sediment samples expressed by $\epsilon_{\text{Nd}(t)}$ (MacLeod et al., 2011; Murphy and Thomas, 2013; Jung et al., 2013; Voigt et al., 2013). A major reorganization of oceanic circulation patterns across the Maastrichtian involves a change in the source of deep-water formation from the tropical areas to high southern latitudes, and implies the onset of a modern-like thermohaline circulation in the Atlantic (Frank and Arthur, 1999; see also Puecat et al., 2005). While the existence of ocean circulation changes is well-documented, their patterns and driving forces are still ambiguous. Another proposed scenario for the perturbation across the MME is related to the global tectonic and magmatic activity such as faster spreading or hotspots (Frank and Arthur, 1999; Voigt et al., 2013; Jung et al., 2013).

2.5. The mid-Maastrichtian global warming episode

The global compilation of $\delta^{18}\text{O}$ and $\delta^{13}\text{C}$ data from Maastrichtian deep-oceanic basins (Barrera, 1994; MacLeod and Huber, 1996; Barrera and Savin, 1999; Li and Keller, 1998; Jung et al., 2013) suggests that these isotopic anomalies were driven by global climate trends likely related to changes in the CO_2 atmospheric concentration (Thibault et al., 2016; Keller et al., 2016; Barral et al., 2017). After a cooling episode in the early Maastrichtian lasting from 71 to 69.5 Ma, a climatic warming

of $\sim 2\text{--}3^\circ\text{C}$ has been inferred worldwide from the record of more depleted $\delta^{18}\text{O}$ values of foraminiferal shells from Pacific, Indian, and South Atlantic oceanic basins (Barrera, 1994; Barrera and Savin, 1999; Li and Keller, 1998; Keller et al., 2016; Jung et al., 2013). This climate warming began at the top of chron C31r (69.5 Ma) and continued until the base of chron C30n (67.5 Ma), so it lasted for ~ 2 Myr. Besides the $\delta^{18}\text{O}$ data, climatic warming was documented by biotic markers such as prominent changes in calcareous nannofossil assemblages of the European Epicontinental Chalk Sea (Thibault et al., 2015, 2016), poleward migration of several low-latitude planktonic foraminifera (Huber et al., 1992) as well as blooms of some disaster opportunist planktonic foraminiferal species in the Indian Ocean, and across the Tethys and Gulf of Mexico (Keller et al., 2016). MacLeod and Huber (1996) noted that the mid-Maastrichtian climate warming event was contemporaneous with inoceramid extinctions in the Southern Hemisphere (MacLeod and Huber, 1996).

3. Material and methods

3.1. Material studied

Two sections with a complete and continuous record of Maastrichtian strata composed of well-preserved carbonate sediments were investigated. The Stevens-1 core is located (Fig. 1) along the coast of Stevns Klint on the eastern shore of Sjælland in Denmark (Stemmerik et al., 2006), close to the historical K-Pg section and type locality for the Danian stage (Surlyk et al., 2006). The Polanówka UW-1 core is situated in eastern Poland. Polanówka UW-1 belongs to the Middle Vistula River valley composite section, the Upper Cretaceous succession of the Polish Basin (Walaszczyk, 2012). Polanówka UW-1 is a 91 m deep borehole drilled and fully cored in 2019 in the frame of this project. PVC pipes (15 cm diameter) were used as protection against core disintegration and contamination. Later, cylindrical samples (3 cm diameter, ca. 4 cm long) were drilled horizontally from the core, assuring high resolution and precision of sampling in the basal 45 m-thick interval

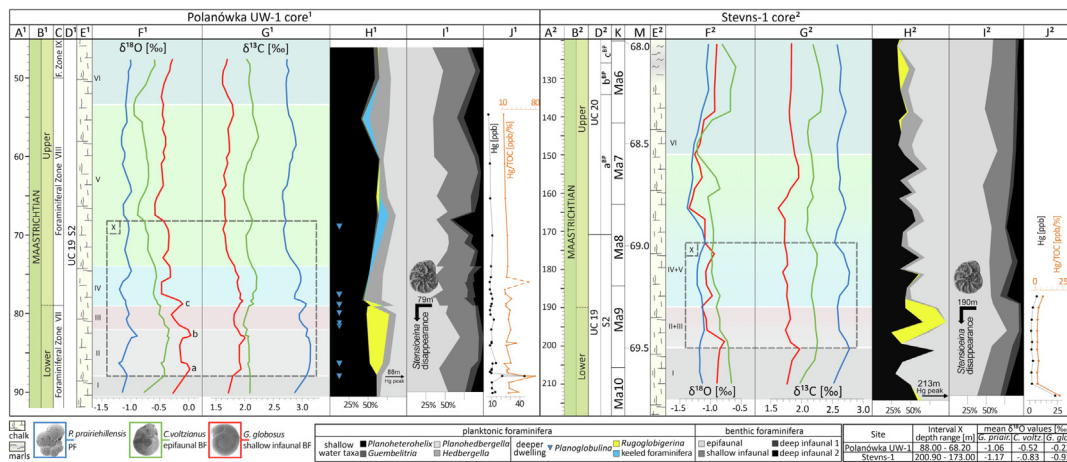


Fig. 3. Correlation of Polanówka UW-1 and Stevns-1 sections on the basis of foraminiferal assemblages, $\delta^{18}O$ and $\delta^{13}C$ curves and Hg concentration. A – depth in meters; B – chronostratigraphy; C – foraminiferal zonation after Dubicka and Peryt, 2012a, b; D – boreal nannofossil zonation after (Boussaha et al., 2016); E – lithological columns; F – three-point moving average curve of $\delta^{18}O$ [‰ V-PDB] measured in foraminiferal shells; G – three-point moving average curve of $\delta^{13}C$ [‰ V-PDB] measured in foraminiferal shells; H – planktonic foraminiferal assemblages; I – benthic foraminiferal assemblages; J – Hg [ppb] and Hg/TOC [ppb/%] in bulk rock samples; K – 405 kyr cycles (Thibault et al., 2012); M – absolute numerical ages [Ma].

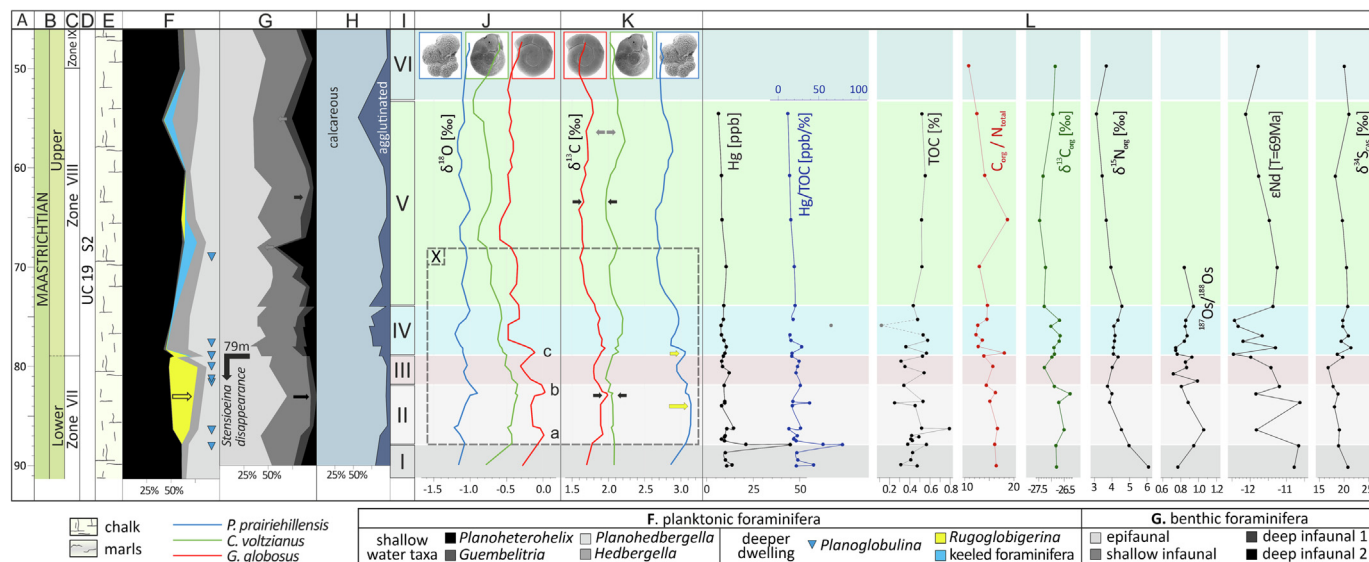


Fig. 4. Foraminiferal assemblages, foraminifera $\delta^{18}O$ and $\delta^{13}C$ curves, Hg concentration, Hg/TOC, TOC, C_{org}/N , $\delta^{13}C_{org}$, $\delta^{15}N_{org}$, $^{187}Os/^{188}Os$, and $\delta^{34}S_{CAS}$ of the Polanówka UW-1 section. A – depth in meters; B – chronostratigraphy; C – foraminiferal zonation after Dubicka and Peryt, 2012a, b; D – boreal nannofossil zonation (Boussaha et al., 2016); E – lithological column; F – planktonic foraminifera assemblages; G – benthic foraminiferal assemblages; H – calcareous/agglutinated benthic foraminiferal ratio; I – geochemical intervals I–VI; J – three-point moving average curve of $\delta^{18}O$ [‰ V-PDB] measured in foraminiferal shells; K – three-point moving average curve of $\delta^{13}C$ [‰ V-PDB] measured in foraminiferal shells; L – geochemical analyses conducted in bulk rock samples.

between 91 and 46 m (Figs. 3, 4). For foraminiferal stable C and O isotopes, the average sampling resolution was 90 cm, which gives an estimate of <10 kyr of temporal resolution. In the critical 5 m-thick interval across the *Stensioeina* extinction (intervals II–IV), the sampling resolution was increased to ~20–50 cm (~2–5 kyr). A total of 44 samples were analysed from the Stevns-1 core. These samples were small rock fragments ~30 cm³ each, collected across a 125 m-thick interval between 213 and 88 m. This interval spans approximately across 69.6 to 67.6 Ma according to the age-model established by (Thibault et al., 2016), thus providing an average sampling resolution of ~3 m, that translates to ca. 50 kyr of temporal resolution. Limited availability of the core material did not allow for collection of larger samples with a higher resolution in Stevns-1. The chalk of the Polanówka UW-1 and Stevns-1 cores is completely bioturbated. Ichnofossils in the Cretaceous chalk show

reworking of the chalk ooze via burrowing to depths of several decimetres below the sea floor (Ekdale and Bromley, 1984; 1991). Therefore, individual samples comprise a mixture of rock matrix and slightly younger material from the infilling of burrows. Consequently, the applied high sampling resolution, especially the interval with ~50 cm sampling resolution, may be associated with a short-term proxy variation resulting from temporal changes affected to some degree by fluctuations in burrowing activity. Hence, a 3-point moving average has been run over the $\delta^{13}C$ and $\delta^{18}O$ data. Since the maximum penetration depth of burrows estimated for Upper Cretaceous decompacted chalk of ~40 cm (Bromley and Ekdale, 1986; Wetzel, 1987) is similar to or lower than the applied sampling resolution (>50 cm), the 3-point moving average surely reflects temporal changes of $\delta^{13}C$ and $\delta^{18}O$ in the basin.

3.2. Foraminifera

A total of 51 samples from Polanówka UW-1 and 42 from Stevns-1 were examined for foraminiferal assemblages and shell geochemistry. Bulk chalk samples (approximate weight of dry sediment was 100 g each) were mechanically disintegrated by soaking in tap water and using Glauber's Salt [$\text{Na}_2\text{SO}_4 \cdot 10\text{H}_2\text{O}$] freeze–thaw method (e.g., Green, 2001). Samples were then cleaned in an ultrasonic bath, wet-sieved through 71 μm mesh and dried at 30 °C in a laboratory dryer.

Benthic (BF) and planktonic foraminiferal (PF) tests were manually picked from the obtained residues using a light microscope Nikon SMZ18 at 100–216x magnification and separated according to the taxonomy to determine the stratigraphic range of individual taxa. A total of 27 samples from Polanówka UW-1 and 22 samples from Stevns-1 were analysed for assemblage composition by counting over 300 specimens. Stratigraphic distribution of all recorded planktonic and benthic foraminiferal species was conducted in both sections. The relative abundances of foraminiferal morphogroups within planktonic and benthic foraminiferal assemblages were calculated separately (Fig. 3H, 3I; Supplementary Table 1).

Three PF assemblages were distinguished according to standard depth-morphogroups (Leckie, 1987; Caron and Homewood, 1983; Hart and Bailey, 1979): (1) shallow-water taxa including biserial heterohelicids (*Planoheterohelix striata*, *P. globulosa*, *Laeviheterohelix glabrans*), triserial guembeltriids (*Guembeltria cretacea*), planispiral *Planohedbergella* (*Planohedbergella prairiehilensis*, *P. aberrantus*, *P. multispina* traditionally assigned to *Globigerinelloides* (see Huber et al., 2022) and trochospiral *Hedbergella*; (2) intermediate water dwelling taxa including *Rugoglobigerina* (*R. pennyi*, *R. milamensis*, *R. rugosa*, *R. macrocephala*) and (3) deep-dwelling water taxa including all keeled foraminifera (*Contusotruncana fornicata*, *C. patelliformis*, *C. plummerae*, *Globotruncana arca*, *G. linneiana*, *G. bulloides*, *Globotruncanita pettersi* and *G. stuartiformis*). Rare specimens of deep-dwelling, complex heterohelicids (*Planoglobulina brazoensis*, *P. carseyae*) were observed throughout the Polanówka UW-1 section (Fig. 5) but their number was insufficient for statistics.

Similar qualitative and quantitative analysis was conducted for major morphogroups of benthic foraminifera. Four main BF assemblages were distinguished (the percentage given next to the generic name indicates content of individual genera among each specific ecological group) according to microhabitat pattern (Corliss and Chen, 1988).

In Polanówka UW-1 section we calculated (1) epifaunal morphogroups represented by very low trochospiral or planispiral, flattened, often plano-convex genera (*Cibicidoides* – 54 %, *Gavelinella* and *Anomallinoides* – 22 %, *Lenticulina* – 10 %, *Stensioeina* – 9 %, *Osangularia* and *Cibicides* – 3 % each, other taxa – 2 %); (2) shallow infaunal morphogroups, including rounded taxa such as *Gyroidinoides* (31 %), *Valvulineria* (8 %), *Pullenia* (8 %), *Lagena* (4 %) and other taxa (10 %), tapered genera including *Pseudovigierina* (13 %) *Praebulimina* (10 %), *Pyramidina* (8 %) *Eovigierina* (4 %) and other (4 %) as well as flattened *Neoflabellina* and *Fronicularia* (1 % each); (3a) deep-infaunal forms including elongated genera such as *Nodosaria* and *Dentalina* (73 %), *Saracenaria* and *Marginulina* (20 %) and others (7 %); and (3b) deep infaunal genera such as *Bolivina* (35 %) and *Bolivinoidea* (7 %) and agglutinated foraminifera including *Gaudryina*, *Heterostomella*, *Textularia*, *Lamina* and others (58 %). In Stevns-1 core we distinguished: (1) epifaunal morphogroups such as very low trochospiral or planispiral, flattened, often plano-convex genera (*Cibicidoides* – 50 %, *Gavelinella* and *Anomallinoides* – 28 %, *Stensioeina* – 7 %, *Lenticulina* – 7 %, *Osangularia* – 6 %, *Eponides* – 1 % and others – 1 %); (2) shallow infaunal morphogroups, including tapered *Praebulimina* (29 %), *Pseudovigierina* (18 %), *Arenobulimina* (8 %) *Pyramidina* (6 %) *Eovigierina* (3 %) and

rounded *Gyroidinoides* (11 %), *Pullenia* (7 %), *Lagena* (5 %) *Valvulineria* (4 %), and other taxa (9 %); (3a) deep-infaunal forms included elongated genera such as *Nodosaria* and *Dentalina* (72 %), *Saracenaria* and *Marginulina* (25 %) and others (3 %); and (3b) deep infaunal genera such as *Bolivina* (42 %) and *Bolivinoidea* (17 %) and agglutinated foraminifera, e.g., *Gaudryina*, *Heterostomella*, *Textularia*, *Ataxophragmium* and others (41 %).

In order to assess potential diagenetic changes of foraminiferal tests, several procedures were conducted. Foraminiferal tests from both studied sections were examined with a light microscope (Nikon SMZ18) and Zeiss Sigma VP field-emission scanning electron microscope (SEM) in order to evaluate shell pores, ornamentations, micro- and nanostructures, possible overgrowths, dissolution, or shell infillings. SEM analysis was conducted at the Faculty of Geology, University of Warsaw (UW); samples were coated either with platinum or carbon. Additionally, elemental composition of foraminifera shells from Polanówka UW-1 was examined using a CAMECA SX 100 electron microprobe (EMP) at the Faculty of Geology UW on polished thin sections (coated with carbon) of 62 specimens of *C. voltzianus* and 24 tests of *G. prairiehilensis*, from 5 stratigraphic levels (86.3 m, 78.9 m, 74.9 m, 65.1 m and 46.1 m). Overall, contents in Na, Mg, Sr, Ca, Ba, Pb, P, S, Fe, Mn, and K were measured in 65 analytical points (27 analytical points in benthic foraminifera shells and 38 in planktonic foraminifera shells). In 16 out of 27 points, in *C. voltzianus* shells, Al and Si contents were additionally measured. Detailed results of the elemental composition are presented in Supplementary Table 2.

For oxygen and carbon isotope analyses, large (adult size) planktonic and benthic calcite foraminiferal tests were manually picked. $\delta^{13}\text{C}$ and $\delta^{18}\text{O}$ values were measured in 279 monospecific samples (153 from Polanówka UW-1 and 126 from Stevns-1), which consisted of three separated species representing different life strategies: planktonic *G. prairiehilensis*, benthic epifaunal *C. voltzianus*, and benthic infaunal *G. globosus*. Every foraminiferal sample contained 20–120 foraminiferal tests of each taxon derived from a specific core depth. Oxygen and carbon isotope analysis of foraminiferal samples was performed at the GeoZentrum Nordbayern, University of Erlangen-Nürnberg, Germany. Samples were reacted with 100 % phosphoric acid at 70 °C using a Gasbench II connected to a ThermoFisher Delta V Plus mass spectrometer. All $\delta^{18}\text{O}$ and $\delta^{13}\text{C}$ values are reported in per mil relative to the VPDB scale and listed in Supplementary Table 3. Reproducibility and accuracy was monitored by replicate analyses of laboratory standards calibrated by assigning $\delta^{13}\text{C}$ values of +1.95 ‰ to NBS19 and –47.3 ‰ to IAEA-CO9 and $\delta^{18}\text{O}$ values of –2.20 ‰ to NBS19 and –23.2 ‰ to NBS18. Reproducibility (1 σ) over the course of analyses of the Polanówka UW-1 samples was better than ± 0.07 ‰ for $\delta^{18}\text{O}$ and ± 0.06 ‰ for $\delta^{13}\text{C}$.

The remaining methods described below were applied to bulk chalk samples.

3.3. Mercury (Hg), total organic carbon (TOC), total sulphur (TS), and calcium carbonate (CaCO_3) contents

A total of 31 chalk samples from Polanówka UW-1 and 10 from Stevns-1 were crushed, homogenized, pulverized (ca. 1 g per sample), and analysed for Hg, total organic carbon (TOC), total sulphur (TS), and CaCO_3 contents at the Institute of Earth Sciences, University of Silesia in Katowice, Poland. The mercury (Hg) contents were measured using a dual-cell pyrolyser-type Milestone DMA-80 Direct Mercury Analyser for atomic absorption spectrometry (AAS). The instrument was calibrated using certified reference material INCT-OBTL-5 (tobacco leaves) prior to the measurement, with Hg content consist 20.9 ppb. The measurement of each sample was duplicated. The detection limit was 0.2 ppb, and analytical details of the analysis were reported by (Racki et al., 2018a). The

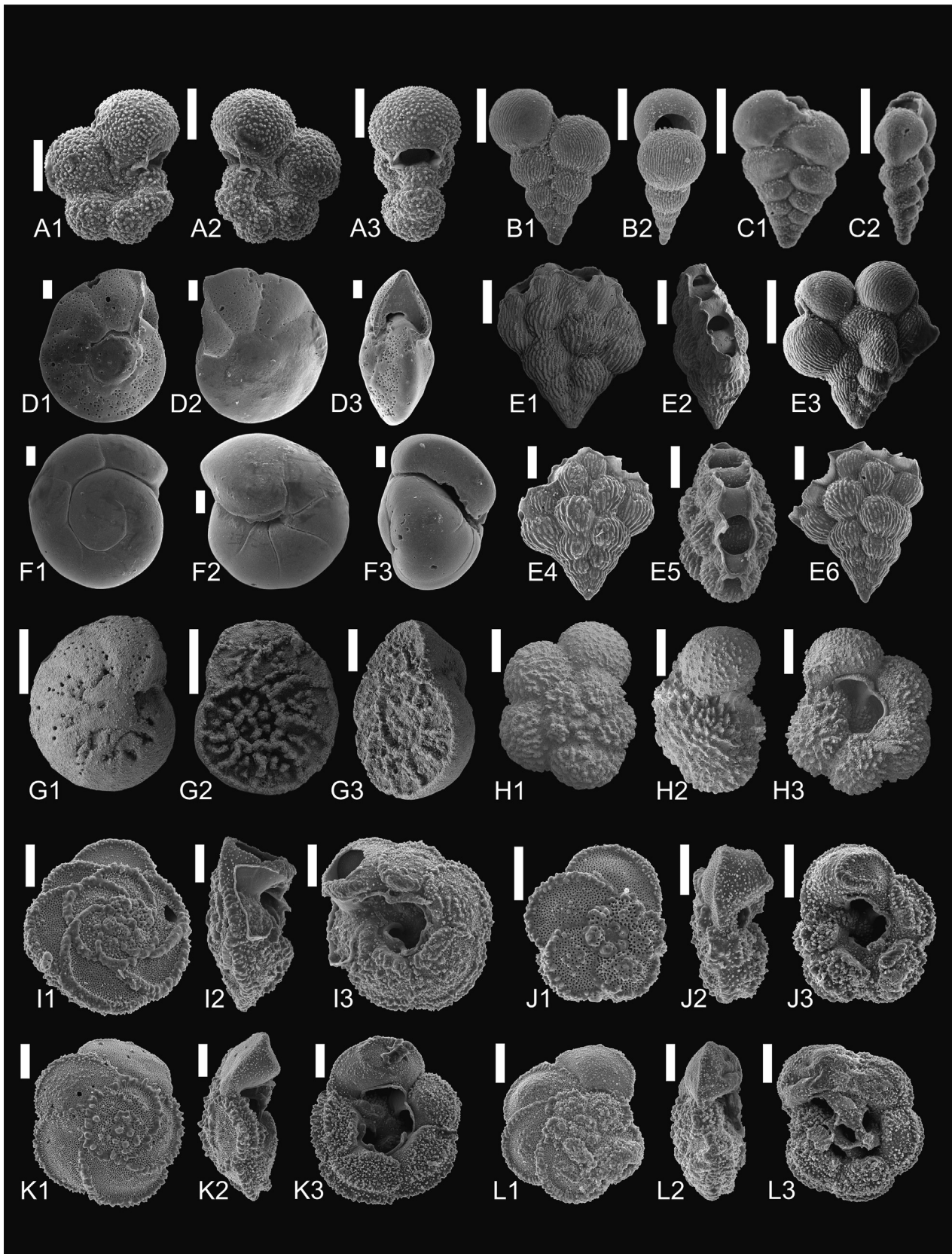


Fig. 5. SEM images (in secondary electrons) of planktonic and benthic foraminifera from Polanówka UW-1. A1-3. *Planohedbergella prariehillensis* (Pessagno 1967), B1-2 *Planoheterohelix striata* (Ehrenberg, 1840), C1-2 *Laeviheterohelix glabrans* (Cushman, 1938), D1-3 *Cibicidoides voltzianus* (d'Orbigny, 1840), E1-6 *Planoglobulina brazoensis* Martin 1972, F1-3. *Gyroidinoides globosus* (Hagenow, 1842), G1-3. *Stensioeina pommerana* Brotzen, 1936, H1-3 *Rugoglobigerina pennyi* Bronnimann, 1952. I1-3 *Globotruncanita pettersi* (Gandolfi, 1955); J1-3 *Globotruncana hilli* Pessagno 1967, K1-3 *Contusotruncana patelliformis* (Gandolfi, 1955), L1-3 *Globotruncana bulloides* Vogler, 1941; scale bars equal 100 μm .

total carbon (TC), total inorganic carbon (TIC), and total sulphur (TS) contents of samples were measured using an Eltra CS-500 IR Analyser which is equipped with a TIC analysis unit. Total carbon (TC) and total sulphur (TS) contents were determined using an infrared cell detector in CO₂ gas, which was evolved by combustion in an oxygen atmosphere. Total inorganic carbon (TIC) contents were derived from a reaction with 15 % hydrochloric acid; CO₂ was determined using an infrared detector. Total organic carbon (TOC) contents were calculated as the difference between the total carbon (TC) and total inorganic carbon (TIC) contents: TOC [wt. %] = TC [wt. %] – TIC [wt. %]. Approximate CaCO₃ [wt. %] contents were calculated as CaCO₃ [wt. %] = TIC [wt. %] × 8.3333. The analytical precision and accuracy were better than ±2 % for TS, ±2% for TC, and ±3 % for TIC. Calibration of the analyser was accomplished using Eltra standards.

3.4. Quantitative XRD

Samples for bulk rock analysis were gently crushed and then ground in a McCrone mill with the addition of methanol and ZnO as internal standard (Śrdoń et al., 2001). Preparation followed a side-loading procedure in order to maximize disorientation of mineral grains. Quantitative mineralogical analysis was performed by matching the diffraction patterns of the test samples with the diffraction patterns of previously recorded pure standards using Q-Min software. In order to prepare clay fractions (<2 μm) samples were treated chemically to remove carbonates, organic matter and iron oxides (Jackson and Barak, 2005) and then the separated fractions were collected by centrifugation. Oriented specimens were prepared by air-dried sedimentation on glass slides followed by intercalation with ethylene glycol. Quantitative analysis of clay minerals was performed using the Sybilla program on glycolated specimens. Phases other than clay minerals were not fitted by the program and diffractograms registered in air-dried conditions were checked for confirmation of the analysis. The analysis was carried out at the Clay Minerals Laboratory, Institute of Geological Sciences, Polish Academy of Sciences (IGS PAS), Cracow.

3.5. Trace element analysis

Rare earth element (REE) and Y contents were determined in bulk chalk samples collected from the Polanówka UW-1 core at the Uranium and Stable Isotopes Laboratory, IGS PAS, Warsaw. Samples underwent dissolution in a weak acetic acid following the protocol of Rongemaille et al., 2011 in order to obtain results for the carbonate fraction. 1 mg of powdered chalk of each sample, carefully weighed and placed in a teflon vial, was digested in 3 ml of 5 % (v/v) ultra-pure acetic acid. The solution was left on mechanical shaker for 24 h at room temperature, then transferred to a pre-cleaned polypropylene tube and centrifuged for 2 min at 2500 rpm to remove undissolved residuum from the solution. Once the supernatant was clear, it was filtered using 0.45 μm syringe filters, transferred to teflon vials, and dried on a hotplate in 180 °C. When acetic acid evaporated the sample was dissolved in 3 ml of 50 % (v/v) twice-subboiled HNO₃. Finally, a few hours before the analysis, 2 ml of prepared solution was evaporated and analyzed in 6 ml of 2 % (v/v) HNO₃.

The concentrations of elements were determined by high resolution inductively couple plasma mass spectrometry (HR-ICP-MS Attom ES Nu Instruments). This instrument is equipped with a MicroMist nebulizer (0.2 ml × min⁻¹) and a Peltier-cooled spray chamber for sample introduction. The optimal signal intensity and stability was achieved in the following, manually optimized, conditions: nebulizer 29.9 PSI; auxiliary 0.80 L × min⁻¹; coolant 13.0 L × min⁻¹. The RF power was set to 1300 W. Concentrations of the REE+Y were determined under low resolution. The determi-

nations by ICP-MS were performed using calibration curves from diluted stock of multi-element standard 10 μg × mL⁻¹ (CMS-1 inorganic ventures). The analytical quality control was verified by the analysis of certified reference material SLRS-6 (National Research Council Canada).

3.6. Content and isotopic composition of N and C in organic matter

After removing carbonates with 1 M HCl, samples were analyzed for δ¹³C_{org} and δ¹⁵N_{org} with a Thermo 1112HT Flash Elemental Analyzer coupled to a Thermo Delta V Advantage IRMS in continuous flow mode, at the Stable Isotope Laboratory, IGS PAS, Warsaw. δ¹³C_{org} and δ¹⁵N_{org} values were normalized against USGS-40, USGS-41, and IAEA-600 standards and reported relative to VPDB and atmospheric nitrogen, respectively. The analytical error of the measurements was up to ±0.3 ‰ for δ¹³C_{org}, and ±0.2 ‰ for δ¹⁵N_{org}. The content of nitrogen and carbon in the undissolved residue was determined using Vario MicroCUBE elemental analyzer. Samples wrapped in tin capsules were combusted at 1150 °C. Released gases (CO₂ and N₂) were separated in GC column and determined by thermal conductivity detector. The content was normalized with reference to sulfanilic acid standard measurements. Results are reported as weight % (wt.%). Measurement precision (1σ) was ±0.6 wt.% for C and 0.18 wt.% for N. Lower limit of detection was 40 ppm for every element.

3.7. S isotope composition of carbonate-associated sulfate (CAS)

CAS extraction was carried out in three steps following the procedure by Theiling and Coleman, 2015 with minor modifications: removal of non-CAS sulfates (Step 1), dissolution of carbonate to liberate lattice-bound SO₄²⁻ (Step 2), and precipitation of sulfate ions as BaSO₄ (Step 3). In Step 1, 5 g of a powdered sample was rinsed three times with 100 ml of 10 % NaCl solution. The supernatant was filtered and 8.5 % BaCl₂ solution was added at pH ≤2. After 24 h barite did not precipitate meaning that all non-CAS sulfate was effectively removed. Then, the material was rinsed three times with deionized water, dried at 60 °C for 24 h, and weighed. Step 2 was carried out in Erlenmeyer flasks in a closed system, maintaining a constant N₂ flux in the flask headspace. Carbonate was dissolved during 90 min-long reaction with 10 % HCl added to the Erlenmeyer flasks from a dropping flask. Upon reaction completion, samples were centrifuged at 4500 rpm for 10 min and the supernatant was decanted and filtered. In Step 3, 8.5 % BaCl₂ solution was added to the supernatants that were kept for 3 h at pH ≤2 and 60 °C with stirring under atmospheric conditions. Then, BaSO₄ precipitated from the solutions during cooling down at room temperature for 72 h. The solutions were filtered and the material left on the filters was rinsed with deionized water, dried for 24 h at 40 °C, scratched off, and placed in Eppendorf vials for δ³⁴S measurements.

Measurements of δ³⁴S in extracted CAS were performed at the Stable Isotope Laboratory, IGS PAS, Warsaw, using a Flash 1112 HT elemental analyzer (Thermo Scientific) coupled with a Delta V Advantage IRMS (Thermo Scientific) in a continuous flow of helium. For δ³⁴S determination, samples were wrapped in tin foil (about 400 μg BaSO₄ mixed with ten times V₂O₅) and combusted at 1020 °C. The obtained SO₂ was then purified on water trap, separated on GC column from other gases and introduced to the mass spectrometer, where its isotopic composition was measured. The results of duplicate analysis were calculated with three international standards: NBS 127, IAEA SO-5, IAEA SO-6 and reported relative to VCDT international standard. The measurement precision (1σ) and reproducibility were generally better than ±0.3 ‰.

3.8. Neodymium isotope composition

The Nd-Sm isotope measurements were performed in the Isotope Laboratory of the Adam Mickiewicz University, Poznan, Poland, on a Finnigan MAT 261 multi-collector thermal ionization mass spectrometer. The powdered carbonate samples (~50–100 mg) were weighed into 50 ml centrifuge tubes, treated with weak (5 %) ultra-pure acetic acid and left on a mechanical shaker for 24 h at room temperature following the selective dissolution procedure recommended by Rongemaille et al., 2011. The obtained solutions were centrifuged to separate the acid-soluble fraction; each residue was washed, dried and weighed to determine the content of the nonleachable fraction. To remove potential fine acid-insoluble particles, the supernatant liquids were passed through a syringe filter with a 0.2 mm PTFE membrane. The filtered solutions were then equilibrated with a mixed ^{149}Sm - ^{150}Nd tracer. Rare earth elements (REE) were stripped from the solutions using the Fe hydroxide co-precipitation method described by (Fanton et al., 2002). Light REEs were separated from matrix elements on 50 μl Teflon columns filled with EICHROM TRU resin (see Pin et al., 1994). Subsequently, Nd and Sm were separated on 2 ml columns packed with EICHROM Ln resin. The details of the analytical procedures are described in (Dopieralska, 2009). Nd and Sm (loaded as phosphate) were measured on rhenium (Re) filaments in a double-filament configuration. Isotopic ratios were collected in dynamic (Nd) and static (Sm) modes on a Finnigan MAT 261 multi-collector thermal ionization mass spectrometer. During this study, the AMES standard yielded $^{143}\text{Nd}/^{144}\text{Nd} = 0.512128 \pm 10$ (2σ , $n = 23$). The $^{143}\text{Nd}/^{144}\text{Nd}$ ratios were normalized to $^{146}\text{Nd}/^{144}\text{Nd} = 0.7219$ and Sm ratios to $^{147}\text{Sm}/^{152}\text{Sm} = 0.56081$. Total procedural blanks were less than 40 pg for Nd, which is negligible with respect to the results. Nd isotope data have been corrected for the age-related effect of ^{147}Sm decay (~69 Ma) and reported in the standard ϵ notation calculated using $^{143}\text{Nd}/^{144}\text{Nd} = 0.512638$ and $^{147}\text{Sm}/^{144}\text{Nd} = 0.1967$ for present-day CHUR (Jacobsen and Wasserburg, 1980).

3.9. Osmium isotope composition

The original procedure for the applied Os isotopic analysis is fully described in Brauns, 2001 and Woodhead and Brauns, 2004. In this work, carbonate-rich samples were processed, which required a modification on how the sample is introduced into the Carius tube. In the first step, a mixed ^{185}Re - ^{190}Os tracer was injected into the Carius tube (pre-spiked). In the second step, a maximum of 0.6 g of material (chalk chips 0.2–0.4 mm large) was added. In the third and most important step, 2 ml of concentrated HCl was very slowly added, holding the Carius tube in an 45° position. The rising of foam in the Carius tube was avoided by gently hitting the glass ampoule against the palm of the hand, which caused the foam bubbles to burst. After all the carbonate was dissolved, the Carius tube was placed in a mixture of ethanol and dry ice until the sample liquid became frozen. Finally, 6 ml of concentrated HNO_3 was added, the Carius tube was sealed and the liquid was equilibrated in the tube over 3 days in an oven at ca. 240°C . Osmium, as the volatile OsO_4 , was then directly distilled from the Carius tubes, condensed on ca. 20 μl of chilled sulfuric acid, and finally collected in 2 ml of 8 N HBr. Osmium was further purified using microdistillation techniques (Birck et al., 1997). Os measurements were performed on a modified Finnigan MAT 261 for negative ions (N-TIMS) in a dynamic mode. Details on mass spectrometry techniques and error propagation procedures are given in Brauns, 2001 and Woodhead and Brauns, 2004. Total procedural blanks amounted to 75 fg Os which is less than 0.5 % of the total Os in the samples which were processed in this work and, hence, negligible. The measurements were carried out at the Lab-

oratory for Isotope Analysis, Curt-Engelhorn-Centre Archaeometry gGmbH, Mannheim, Germany.

4. Results

4.1. Biotic changes

In both successions, Polanówka UW-1 and Stevns-1, benthic and planktonic foraminifera are diverse and abundant. Qualitative and quantitative analysis of foraminiferal assemblages from both successions revealed six foraminiferal bioevents in Polanówka UW-1 and five in Stevns-1. In Polanówka UW-1, the first bioevent is the appearance of complex heterohelids of the genus *Planoglobulina* between 88 and 66 m (Fig. 3H1, 4F marked with a blue triangle). Their abundance is rather low, several specimens per sample, therefore they were not included in quantitative studies. Nevertheless, in the interval 78–82 m *Planoglobulina* tests were noted in almost every sample analyzed. The second bioevent is the bloom of *Rugoglobigerina* observed at ca. 88–79 m (Fig. 3H1, 4F, marked in yellow). Representatives of planktonic *Rugoglobigerina* occur from 88 up to 46 m, but within interval 87–79 m they constitute up to 30 % of all planktonic species. Upwards the succession, the contribution of this taxon to the overall assemblage is insignificant except for a minor increase up to 4 % around 65 m. The third bioevent is related to a significant reduction in the proportion of deep-infaunal foraminifera to the overall number of benthic species that occurs around 86–79 m. Across the section, deep-infaunal morphotype abundance represents an average of 18 % of all benthic foraminifera. In the mentioned interval, it drops to as low as 6 % at 83 m (similar decrease of infaunal foraminifera contribution is also observed around 62.5 m where they amount to 7 %). The disappearance of the representatives of the genus *Stensioeina* at 79.02 m is another important foraminiferal event (the fifth) documented (Fig. 3I, 4G, 6F, marked with a black arrows). Before the event, in the lower part of Polanówka UW-1 section, it constitutes an average of 17 % of all epifaunal foraminifera (9 % of all benthic taxa), with a maximum of 33 % among epibenthic foraminifera (16 % of all benthic genera). The sixth bioevent observed in Polanówka UW-1, is the appearance of keeled foraminifera (*Globotruncana* and *Globotruncanita*) in two intervals, between 73 and 66 m and 59–51 m, where they constitute a significant share among all planktonic species, up to 13 and 8 %, respectively. Individual, statistically insignificant juvenile specimens of planktonic keeled foraminifera discontinuously occur throughout almost the entire Polanówka UW-1 section (90.25–49.90 m). In contrast, shallow-dwelling species *Planoheterohelix*, *Planohedbergella*, *Hedbergella*, and *Guembelitria* occur within the entire succession making up respectively 40–64 %, 14–35 %, 4–26 %, <1–6 % of the planktonic foraminiferal assemblages.

In Stevns-1, the biotic events recorded are (1) a bloom of *Rugoglobigerina* between 196 and 190 m (Fig. 3H2) coinciding with (2) a significant reduction in the proportion of deep-infaunal foraminifera to the overall number of benthic species, followed by (3) the disappearance of benthic *stensioeina*ids at 190 m (Fig. 3I2) and (4) the onset of the domination of shallow-water biserial heterohelids within planktonic species at ca. 110 m (Fig. 6F2). *Rugoglobigerina* occurs in the lowermost part of the section to ca. 110 m with two statistically significant episodes: a bloom from 196 to 190 m, where it contributes as much as 30–40 % of all planktonic taxa, and a less frequent occurrence in the interval 140–110 m, persisting to around 2 % with a maximum value of 14 % at 127 m. Shallow surface dwelling taxa, such as *Planoheterohelix* (25–81 % among planktonic foraminifera), *Planohedbergella* (4–70 %) and *Hedbergella* (<1–29 %), occur throughout the entire succession. At 190 m, we observed the last occurrence of *Stensioeina*.

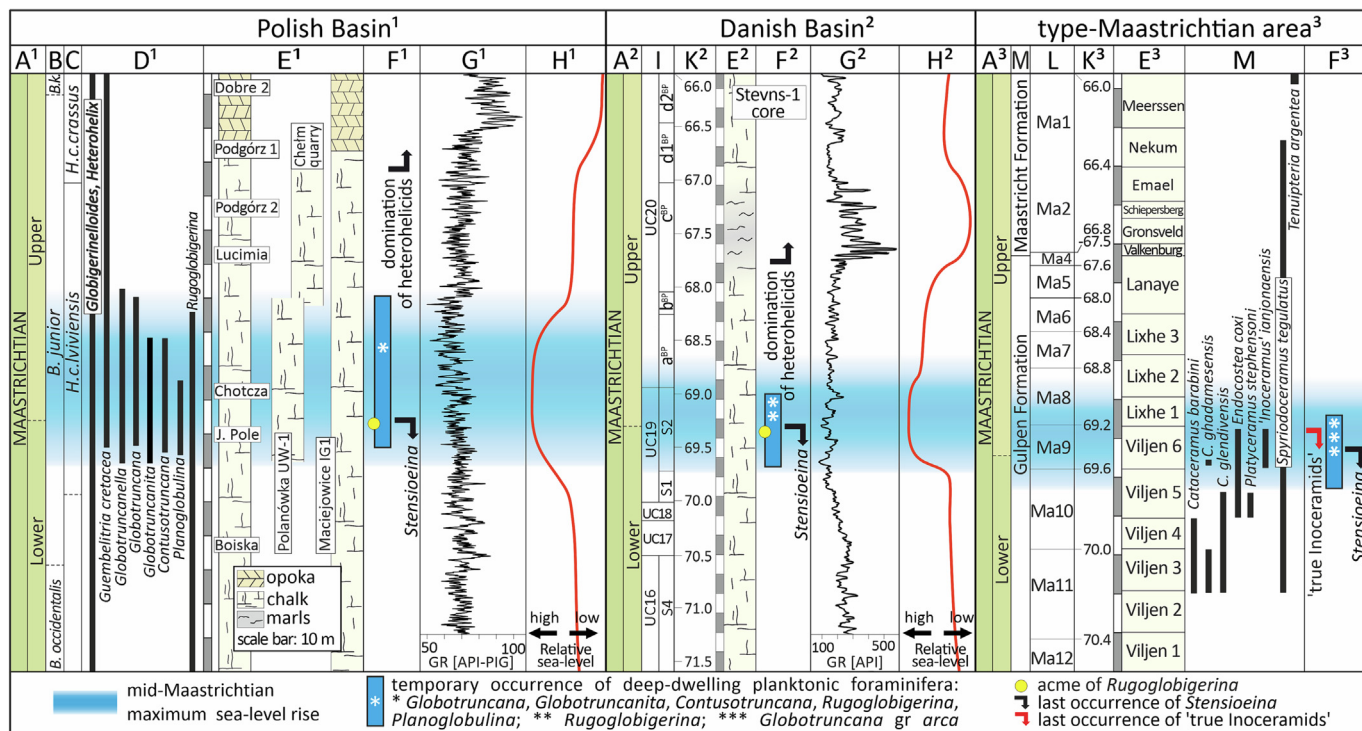


Fig. 6. Correlation of the biotic events recorded in Polish and Danish basins and type-Maastrichtian area. 1 – Dubicka and Peryt, 2012a; Peryt et al., 2022; Becker et al., 2023; this paper; 2 – (Thibault et al., 2012; Surlyk et al., 2013; this paper; 3 – (Keutgen, 2018), Robaszynski et al., 1985; Walaszczyk et al., 2010. A – chronostratigraphy; B – belemnite division (Błaszkiwicz, 1980); C – ammonite zonation (Machalski, 2005); D – foraminiferal ranges (Peryt et al., 2022; this paper); E – lithological columns (scale bar: 10 m); F – bio-events; G – gamma-ray profile [API]; H – sea-level changes; I – boreal nannofossil zonation (Boussaha et al., 2016); L – 405 kyr cycles; K – absolute numerical age [Ma]; M – inoceramid vertical ranges.

Below this depth, *Stensioeina* contributes on average to 26 % of all epifaunal foraminifera (15 % of all benthic taxa), with a maximum value of 29 % of epibenthic foraminifera (22 % of all benthic genera).

In summary, the prominent foraminiferal events that are well visible in both studied sections are: (1) the appearance of deep-dwelling foraminifera, (2) an acme of *Rugoglobigerina* that coincide with (3) the reduction in the proportion of deep-infaunal foraminifera within benthic foraminiferal assemblages and (4) the disappearance of the *Stensioeina* group (*Stensioeina pommerana* Brozten, *S. bella* Gawor-Biedowa and *S. pulchra* Gawor-Biedowa).

4.2. Foraminiferal shell preservation: SEM and elemental analysis

Foraminiferal shells obtained from Polanówka UW-1 core are characterized by an exquisite state of preservation. They are not filled by any sediment, the pores remain open, they do not exhibit overgrowth on either internal or external shell surfaces (Fig. 5), and they possess original test nanotextures (see Dubicka et al., 2018; Dubicka, 2019). In addition, chemical composition of the shells corresponds to that of the modern tests (Dubicka et al., 2018) which attests for their excellent preservation. Sr content in the planktonic *P. prairiehillensis* varies from 0.064 to 0.273 wt.% (Sr/Ca ratio between 0.72 and 3.31 with an average value of 1.50 mmol/mol) while in the benthic *C. voltzianus* it varies from 0.042 to 0.298 wt.% (Sr/Ca ratio between 0.49 and 3.48 with an average value of 1.72 mmol/mol). Na content in the *P. prairiehillensis* varies from 0.037 to 0.131 wt.% (Na/Ca ratio between 0.15 and 0.59 with an average value of 0.36 mmol/mol) and from 0.039 to 0.149 wt.% (Na/Ca ratio between 1.73 and 6.65 with an average value of 3.36 mmol/mol) in *C. voltzianus*. Mn and Fe concentrations, which are indicative of diagenetic alteration in calcite if elevated (Barbin,

2013; Ullmann and Korte, 2015), are below the lower detection limits of the electron microprobe WDS analysis (\leq ca. 0.05 wt.% for Mn which are equivalents of Mn/Ca \leq ca. 0.07 mmol/mol, and \leq ca. 0.04 wt.% for Fe which are equivalents of Fe/Ca \leq ca. 0.9 mmol/mol) in most of the analytical points of both planktonic *P. prairiehillensis* and benthic *C. voltzianus*.

Specimens from Stevns-1 are also empty, with open pores and original nanotextures, however, they display some overgrowth indicating that they are somewhat of a lower quality, but still reasonably well-preserved. Stevns-1 foraminifera were more challenging to treat during the cleaning process, as some tests were slightly overgrown. In order to demonstrate similarities between the sections, we will only focus on results of the Stevns-1 section within the interval of 213–120 m, as the formations above this depth lie outside the stratigraphic range represented in the Polanówka UW-1 section.

4.3. $\delta^{13}C$ and $\delta^{18}O$ curves

Polanówka UW-1 section, can be divided into five intervals characterised by various geochemical trends: >88 m (interval I), 88–82 m (interval II), 82–79 m (interval III), 79–74 m (interval IV), 74–57.5 m (interval V), and <57.5 m (interval VI) (Fig. 4).

The $\delta^{13}C$ values measured in foraminiferal shells of both successions are consistently higher for planktonic taxa than for epibenthic ones, which are in turn higher than those for endobenthic foraminifera (Fig. 3G1, 3G2). The $\delta^{13}C$ values of planktonic *P. prairiehillensis* range from 2.6 to 3.2 ‰ in Polanówka UW-1, and from 2.1 to 2.9 ‰ in Stevns-1. The $\delta^{13}C$ values of epifaunal *C. voltzianus* range from 1.9 to 2.3 ‰ in Polanówka UW-1, and from 1.9 to 2.1 ‰ in Stevns-1. For infaunal *G. globosus*, the $\delta^{13}C$ values range from 1.5 to 2.1 ‰ in Polanówka-UW1, and from 1.2 to

2.4 ‰ in Stevns-1. Standard deviations of $\delta^{13}\text{C}$ values in Polanówka UW-1 are 0.17 ‰ for *G. prairiehillensis*, 0.10 ‰ for *C. voltzianus* and 0.14 ‰ for *G. globosus*, while in Stevns-1 0.18 ‰, 0.14 ‰ and 0.20 ‰, respectively.

The planktonic $\delta^{13}\text{C}$ curves rise in interval I, fluctuate in intervals II and III superimposed to a general decreasing trend, increase in interval IV, followed by a decrease, and then increase in interval V, to decrease again in interval VI in both sections. A similar pattern is observed for the infaunal $\delta^{13}\text{C}$ curve in Polanówka UW-1 and the epifaunal $\delta^{13}\text{C}$ curve in Stevns-1. Contrasting with the latter trends, the infaunal $\delta^{13}\text{C}$ curve is mostly invariant across intervals II–IV in Stevns-1, whilst the epifaunal $\delta^{13}\text{C}$ curve in Polanówka UW-1 is invariant in intervals I–III. The highest $\delta^{13}\text{C}$ values in Polanówka UW-1 are observed in interval II, where the planktonic $\delta^{13}\text{C}$ curve displays a positive excursion of <1 ‰ amplitude. The epifaunal and infaunal $\delta^{13}\text{C}$ curves converge upsection from interval I to II, approach each other at the top of interval II (~83 m), then diverge through interval III, and remain separated from each other by ~0.4 ‰ towards the top of Polanówka UW-1. The planktonic $\delta^{13}\text{C}$ curve in Stevns-1 is less variable, but the highest values are also observed in the basal part of the section around the transition from intervals I to II. The epifaunal and infaunal $\delta^{13}\text{C}$ curves in Stevns-1 are close to each other only in interval I and then remain separated by ~0.4 ‰.

The $\delta^{18}\text{O}$ values measured in foraminiferal shells of both sections are lower for planktonic than for benthic foraminifera (Fig. 3F1, 3F2). The $\delta^{18}\text{O}$ values of infaunal *G. globosus* are lower than those of epifaunal *C. voltzianus* in Stevns-1, while in contrast, $\delta^{18}\text{O}$ values of *G. globosus* in Polanówka UW-1 are enriched in the heavy isotope as compared to values of *C. voltzianus*. The $\delta^{18}\text{O}$ values of planktonic *P. prairiehillensis* range from –1.5 to –0.8 ‰ in Polanówka UW-1 and from –1.5 to –0.8 ‰ in Stevns-1. The $\delta^{18}\text{O}$ values of epifaunal *C. voltzianus* range from –1.5 to –0.3 ‰ in Polanówka UW-1 and from –1.4 to –0.1 ‰ in Stevns-1. Infaunal *G. globosus* $\delta^{18}\text{O}$ values range from –0.7 to 0 ‰ in Polanówka UW-1 and from –1.6 to –0.3 ‰ in Stevns-1. Standard deviations of $\delta^{18}\text{O}$ values for *G. prairiehillensis*, *C. voltzianus* and *G. globosus* are 0.12 ‰, 0.22 ‰, and 0.21 ‰ in Polanówka UW-1, while they are 0.17 ‰, 0.23 ‰ and 0.28 ‰ in Stevns-1, respectively.

The $\delta^{18}\text{O}$ curves of planktonic foraminifera are relatively stable across both successions, whereas the epifaunal and infaunal values exhibit much higher variability. The general trends in the $\delta^{18}\text{O}$ curves of both epifaunal and infaunal foraminifera show an increase and relatively high $\delta^{18}\text{O}$ values in the basal parts (intervals I and lowermost II) in both sections. Then, they decrease across intervals II–V to approach the planktonic values at ~65 m in Polanówka UW-1 and ~150 m in Stevns-1. Above, they diverge from the planktonic values and rise across intervals V–VI. The highest $\delta^{18}\text{O}$ values are observed for benthic foraminifera in the basal parts (intervals I or II), with only insignificantly higher values in VI for the epibenthic ones in Stevns-1. The difference in $\delta^{18}\text{O}$ between benthic and planktonic taxa is in general higher in Polanówka UW-1 than in Stevns-1, especially with regard to the infaunal benthic taxon.

All isotopic curves exhibit higher variabilities in Polanówka UW-1 than in Stevns-1. However, some differences between the two sections may be related to the lower sampling resolution at Stevns-1 in comparison with Polanówka UW-1. High-resolution sampling in Polanówka UW-1 in intervals II–IV revealed three short-lived isotopic events (a–c) at around 87, 83 and 79 m characterized by rather small amplitudes but distinct positive excursions in $\delta^{18}\text{O}$ and $\delta^{13}\text{C}$ for infaunal *Gyroidinoides*. The anomaly at 83 m (event b) coincides with a similar positive $\delta^{18}\text{O}$ excursion in the planktonic values, whereas the anomaly at 79 m (event c) coincides with a similar positive $\delta^{13}\text{C}$ excursion in planktonic values.

4.4. Mercury (Hg), total organic carbon (TOC), total sulphur (TS), and CaCO₃ contents

In Polanówka UW-1 (Fig. 4L), Hg content is relatively low with background levels of ~9.7 ppb (ranging from 6.4 to 13.7). However, in two samples (at ~88 m depth) the Hg and Hg/TOC rise above background levels. Hg contents yielded values of 21.2 to 45.0 ppb, while Hg/TOC (ppb/%) in these two samples reached higher values ranging from 55.82 to 79.7 ppb/% with background levels ca. 22 Hg/TOC (ppb/%). In Stevns-1, Hg contents range from 1.3 to 23.1 ppb with background levels of 2.1 ppb. The Hg/TOC values ranged from 1.7 to 22.3 (ppb/%). The mercury contents and Hg/TOC spikes occur in the lowermost sample (~213.05 m depth) rising to 23.1 ppb and 22.3 ppb/%, respectively. TOC in Polanówka UW-1 ranges from 0.12 to 0.79 wt.% with mean levels ca. 0.47 wt.%, while in the Stevns-1 core, TOC ranges from 0.73 to 1.1 wt.%, with mean levels of ca. 0.93 wt.%.

4.5. Mineral composition based on quantitative XRD

Quantitative XRD analysis was carried out on five samples encompassing intervals I and II of Polanówka UW-1 section. Contents of identified phases was constant: calcite (85.3 ± 0.90 wt.%), clay minerals (8.8 ± 0.83 wt.%), opal CT (4.2 ± 0.72 wt.%), quartz (1.6 ± 0.32 wt.%), and pyrite (0.2 ± 0.13 wt.%) (Table 1). Siliciclastic components, quartz and clay minerals, comprise 8.8–11.8 wt.%. Quantitative XRD analysis of separated clay fraction <2 μm was performed after carbonate removal. The ratio of kaolinite versus the sum of illite, illite–smectite and smectite in the undissolved residue varied from 1.5 to 1.9 % in the basal 6.5 m and dropped to 0.9 % at the transition from interval II to III.

4.6. C/N ratio and rare earth elements

In Polanówka UW-1, C/N ratio (Fig. 4L) in acid-insoluble residue varies from 10.8 to 18.7 and decreases gradually upsection from interval I (16.2 ± 0.22) to V (13.8 ± 2.96). REE+Y distribution in carbonate fraction show a seawater-like pattern in intervals II through V. These twelve samples show an increasing trend from LREE to HREE reflected in high Lu/La ratio (~2.0 ± 0.31), a negative Ce anomaly (Ce/Ce* = ~0.52 ± 0.052), a positive Eu anomaly (Eu/Eu* = ~1.13 ± 0.092), and high Y/Ho ratio (~4.3 ± 8.6). Samples from interval I (two samples analyzed) exhibit a weaker seawater-like pattern with a weaker Ce anomaly (Ce/Ce* = 0.60 and 0.74), lower Y/Ho ratio (32 and 33), and lower ΣREEY than in the overlying intervals.

4.7. Stable nitrogen, carbon and sulfur isotopes in the organic fraction

In Polanówka UW-1 the $\delta^{13}\text{C}_{\text{org}}$ values are uniform ~–26.7 ± 0.30 ‰ (from –27.3 to –26.1 ‰, $n = 20$) (Fig. 4L). A vague decreasing trend can be observed in intervals I–IV and even less distinctive increasing trend in interval V, with minor fluctuations of <1 ‰ amplitude. The $\delta^{15}\text{N}_{\text{org}}$ values drop abruptly from a peak value of 6.1 ‰ at the base of the section to ca. 3.7 ‰ at the top of interval II, and then vary insignificantly around 4.0 ± 0.39 ‰ (3.1 to 4.6 ‰; $n = 14$) in intervals III–V. A vague increasing trend occurs in intervals III–IV and a decreasing trend in interval V, with the inflection point at 4.6 ‰ at the transition from interval IV to V. The $\delta^{34}\text{S}_{\text{CAS}}$ values fluctuate between 16.7 and 21.4 ‰ (~19.5 ± 1.23 ‰; $n = 20$). They drop by ~4 ‰ in intervals I–III, rise back to ~20 ‰ at the transition to interval IV, and remain relatively stable upsection through intervals IV and V. In Stevns-1, only three $\delta^{13}\text{C}_{\text{org}}$ measurements were successful (ranging from –26.4 to –25.3 ‰) due to the insufficient quantity of material remaining after previous geochemical investigations. The $\delta^{15}\text{N}_{\text{org}}$ values were measured

Table 1

Mineralogical composition based on XRD (in wt.%) for bulk-rock samples and separated clay fractions. Il – illite, Il-Sm – mixed-layer illite-smectite, Sm – smectite.

Sample	Bulk-rock samples								Clay fractions [$<2 \mu\text{m}$]							
	Quartz	Calcite	Opal CT	Pyrite	Clinoptilolite	Kaolinite	Il-Sm + Sm	Chlorite	SUM	Il-Sm	Illite	Smectite	Chlorite	Kaolinite	SUM	Kaolinite/(Il + Il-Sm + Sm)
Pol-G-21	1.8	84.3	4.9	0.3	2.6	0.2	5.7	0.2	100	47.4	49.5	0.7	1.5	0.9	100	0.9 %
Pol-G-24	1.6	86.3	3.5	0.1	2.5	0.2	5.6	0.2	100	34.7	60.0	1.3	2.6	1.4	100	1.5 %
Pol-G-26	1.2	86.2	4.7	0.3	1.8	0.2	5.4	0.2	100	47.2	48.1	1.0	1.9	1.8	100	1.9 %
Pol-G-27	2.0	84.8	3.3	0.1	2.8	0.2	6.6	0.2	100	45.8	50.0	0.7	2.0	1.5	100	1.6 %
Pol-G-28	1.4	84.9	4.4	0.0	2.6	0.2	6.3	0.2	100	49.0	46.9	1.0	1.3	1.8	100	1.9 %

in the basal part of the section. They oscillate around 4.1 ‰ with a negative excursion down to 2.5 ‰ at 213.05–203.9 m and with a rise up to 5.5 ‰ at 196–187 m. $\delta^{34}\text{S}_{\text{CAS}}$ was not analyzed for Stevns-1 samples.

4.8. Radiogenic isotope compositions

Nd and Os isotopes were analyzed only in the Polanówka UW-1 core. The $\varepsilon_{\text{Nd}(t)}$ values fluctuate between –12.5 and –10.6 ($\sim -11.6 \pm 0.56$; $n = 20$). In intervals I–IV they decrease by almost 2 ε units to –12.4 at 75.4 m, then rise abruptly to –11.4 at the transition to interval V at 74 m, and remain relatively stable in the uppermost interval V (spread of $<0.8 \varepsilon$ unit). In interval II, high-frequency fluctuations with an amplitude of about 1 ε unit are observed. Osmium isotopes were measured in intervals I–IV and in the basal part of interval V (>70 m) of the Polanówka UW-1 section in order to achieve a high temporal sampling resolution for this critical interval. The $^{187}\text{Os}/^{188}\text{Os}$ values vary in a broad range of values across 0.72–1.06 ($\sim 0.86 \pm 0.089$; $n = 19$). They exhibit a positive excursion with an amplitude of 0.3 across intervals I–II (1.06 being the peak value), then fluctuate around lower-range values in intervals III and lower part of IV up to 78 m ($\sim 0.82 \pm 0.098$; $n = 8$), and continue on an average level ($\sim 0.87 \pm 0.039$; $n = 6$) at the transition from interval IV to V (78–70 m).

5. Discussion

5.1. Eustatic sea-level rise

The appearance of deep-dwelling planktonic foraminifera in Polanówka UW-1 core, represented by large, complex-keeled forms such as *Contusotruncana*, *Globotruncana*, *Globotruncanita* and *Globotunconella* (Caron and Homewood, 1983; Leckie, 1987; Isaza-Londoño et al., 2006), and the appearance of intermediate surface-dwelling taxa *Rugoglobigerina* in both studied sections (Fig. 3H1, 3H2), indicate a significant sea-level rise at that time. Differences in planktonic foraminiferal assemblages between Polanówka and Stevns-1 reflect the different water depths and paleolatitudinal positions of both localities. Stevns-1 represented a shallower environment than that at Polanówka according to their planktonic foraminiferal assemblages, that of Stevns lacking the deepest dwelling keeled forms. The MME-related transgression corresponds to the global transgressive peak no. 4 of Hancock (1993) recognized in the proximity of the lower–upper Maastrichtian boundary, i.e. within the lower part of the *Belemnitella junior* Zone in western and central Europe (Hancock, 1989; Dubicka and Peryt, 2012a, b) as well as in North America (South Dakota and Atlantic coastal plain, Hancock, 1993).

Keeled globotruncanids (*Globotruncana*, *Globotruncanita*, *Contusotruncana*) were not observed in the Central European Basin following the upper part of the Campanian (Peryt, 1980; Peryt et al., 2022). After their occurrence within the relatively short-

lived mid-Maastrichtian interval, they rapidly disappear in the lower part of the *B. junior* Zone (Dubicka and Peryt, 2012a, b). The latter observation indicates that the observed amplitude of the sea-level rise was high, of at least several dozen meters but probably closer to ~ 100 m, as indicated by calculations based on planktonic foraminiferal markers (Caron and Homewood, 1983; Leckie, 1987). Estimations of maximum sea-level rise during the Maastrichtian range between 50 and 70 m (Olsson, 1988; Kominz et al., 2008; Ray et al., 2019), which coincides with our estimation.

After the sea-level rise observed within the UC19 nanofossil zone and Ma9 astronomical cycle, the onset of a regressive phase is marked by the domination of shallow-water taxa such as small, biserial heterohelicids (e.g., *Planoheterohelix striata*, *P. globulosa*, *Laeviheterohelix glabrans*) (Fig. 6F1, 6F2) within planktonic foraminiferal assemblages in Stevns-1 at 110 m and in Podgórz of the Vistula River section (Dubicka and Peryt, 2012a). This event is followed by positive excursions in gamma ray curves (Fig. 6G1, 6G2) documented for the Maciejowice IG1 section (Becker et al., 2023) and Stevns-1 (Thibault et al., 2012; Surlyk et al., 2013) within the UC20b-c^{BP} subzones and C30n magnetochron, likely linked to an input of terrigenous material and coinciding with lithological changes from chalk to opoka in the Vistula Valley (Fig. 6E1, 6E2) (Pożaryski, 1948; Walaszczyk, 2004).

The mid-Maastrichtian sea-level highstand lasted ~ 2 Myr, as constrained by the age-model established for Stevns-1, based on its correlation with the astronomically-dated ODP Site 762C (Thibault et al., 2012; Fig. 6K). The 2 Myr duration of the recorded eustatic event and its high amplitude hardly fit to the short-term eustatic sea-level cycles of $\leq 10^5$ yr (Ray et al., 2019; Sames et al., 2020) corresponding either to 100 kyr glacial-interglacial cycles or to sea-level fluctuations possibly related to 405 kyr oscillations in humidity and the water cycle in the aquifer-eustasy model of Sames et al., 2020.

The magnitude of sea-level changes of more than 50 m is comparable to that of the Permo-Carboniferous glaciation on Gondwana (Isbell et al., 2003) or Cenozoic glaciation on Antarctica (Miller et al., 2020). Modern Earth's ice sheets store water equivalent to 64 m of sea-level. Accordingly, along with an isostatical compensation, the global mean sea level should rise by ~ 45 m in an ice-free world (Conrad, 2013). However, neither glacially-influenced sediments nor landforms in the Maastrichtian of the southern realm have been documented (Ray et al., 2019). Palynological evidence support Maastrichtian mean annual temperatures of ~ 10 – 15 °C for lowlands and mid-altitudes and ~ 5 – 8 °C for higher altitudes in the subalpine to alpine zone of the Antarctic Peninsula (Bowman et al., 2014), which seems to exclude a glacio-eustasy scenario for the mid-Maastrichtian sea-level rise. Modelling simulations taking into account continental configurations seem to allow for the inception of Antarctic ice-sheets, with growth and decay following orbital periods, under CO_2 concentrations of 560 ppm (Ladant and Donnadieu, 2016).

A potential aquifer-eustasy scenario would imply cooling associated with a sea-level rise due to the oceanic release of water stored on land during warm humid greenhouse periods (Föllmi, 2012; Sames et al., 2020). This scenario seems unlikely for the MME due to the lack of evidence for climatic cooling in our dataset (see also Thibault et al., 2016) as well as in other published data showing instead a global climate warming during the mid-Maastrichtian (across C31r–C31n zones) (e.g., MacLeod and Huber, 1996; Barrera and Savin, 1999; Bowman et al., 2014; Salazar-Jaramillo et al., 2016). Moreover, the pollen-spore assemblage (Kumar, 2019) of the transgressive Corsicana Clay of Texas (USA), that corresponds to the mid-Maastrichtian transgressive peak no. 4 (Hancock, 1993), indicates a humid tropical to subtropical climate.

Geotectonic-related processes have a strong influence on global sea-level change by changing the morphology of the ocean-floor and subsequently the volume of ocean basins, for instance via (1) ridge expansion related to faster seafloor spreading, (2) expansion of continental areas, or net dynamic uplift of the seafloor by mantle flow, or (3) oceanic floor volcanic eruptions leading to emplacement of submarine large igneous provinces (LIPs) (Müller et al., 2008a). An increase of oceanic ridge volume in the middle Maastrichtian does not seem a likely explanation due to the vast amount of time (at 10 to 100 Myr timescales) required for such a process to influence the global sea-level (Conrad, 2013). It is worth mentioning, however, that Gurnis' (1990) model includes global sea-level changes of tens of meters during only a few million years, assuming a very fast spreading rate.

A more likely scenario that would better fit the short duration of the mid-Maastrichtian perturbations would be the production of vast oceanic plateaus (at least $\sim 10^6$ km²) with thickened oceanic crust formed from rapidly erupting lava in less than 2–3 Myr (Kerr, 2005). This duration would match better that of the mid-Maastrichtian sea-level rise and climate warming (Keller et al., 2016). Production of oceanic plateaus induces significant sea-level rise (Müller et al., 2008b) as the present-day LIPs elevate sea-level by ~ 100 m. Large-magnitude basalt-dominated LIP activity has recurrence intervals of 10^3 – 10^4 years (Bryan et al., 2010), while felsic eruptions up to 10^5 years are intense ($\sim 10^{11}$ kg s⁻¹) and short-lived (durations of hours to days). For instance, one of the largest known LIPs, the Paraná–Etendeka, was an active site of felsic eruptions over a ca. 1 Myr period at around 132 Ma (Bryan et al., 2010; Brown et al., 2014).

Estimations of Cretaceous sea-level trends related to emplacement and erosion of LIPs have not been constrained so far, nevertheless, it is believed that igneous activity during the Cretaceous was intensive and must have influenced sea level as well as oceanic circulation patterns (Kerr et al., 2000; Kerr, 2005). Because the volume of either ocean ridges or Cretaceous conjugate oceanic plateau was partially lost during the Laramide subduction, the study of Cretaceous tectonic activity is hindered (Liu et al., 2010).

Keller et al., 2016 correlated the ~ 69.5 – 67.5 Ma time interval with a major volcanic activity at DSDP Site 216 on the Ninetyeast Ridge (Kerguelen hotspot) and this interval matches the mid-Maastrichtian sea-level rise. It is worth noting that phase 1 of Decan volcanism also began somewhere around this time (Keller et al., 2016) and might have contributed to mid-Maastrichtian environmental perturbations. Other potential candidates for being a trigger force of the MME are oceanic plateaus Moud Rise and Sierra Leone Rise events dated to ca. 73 Ma (Eldholm and Coffin, 2000).

Although the general global estimates of ocean spreading rates are low for the Maastrichtian, the late Maastrichtian is characterized by an increase (including the North Atlantic), which is especially significant in the Indian ocean (Larson, 1991; Cogné and Humler, 2006). Finally, during the mid-Maastrichtian, seafloor

spreading around Australia was also an active process, including the onset of seafloor spreading in the northern Tasman Sea (Müller et al., 2000).

Volcanism and hydrothermal activity are considered as the main sources of Hg in sedimentary rocks (e.g., Sial et al., 2010; Sanei et al., 2012; Grasby et al., 2019). In the Polanówka UW-1 core Hg values reach 45 ppb (at 88 m), which is >4.5 times higher than the background level, while in the Stevns-1 core, the Hg spike reaches 23.1 ppb (in the lowermost sample at ca. 213 m), which is >11 times higher than the background level in this section. Many studies emphasized the strong affinity of Hg to organic matter (OM). Therefore, normalisation to total organic carbon (TOC) has often been used to decipher significant Hg enrichments from biased spikes related to enhanced OM deposition (e.g., Sanei et al., 2012; Grasby et al., 2019). The Hg/TOC anomalies correspond closely with the identified Hg spikes in both sections examined. The Hg/TOC ratio in Polanówka UW-1 is 3.5 times higher, whereas in Stevns-1 it is 11 times higher than the background level (=median value). In Polanówka UW-1, one sample (at 76 m) yielded a high Hg/TOC value of 65.8 (ppb/%), which is considered as unreliable, because the TOC value is very low (<0.2 wt.%) in this sample (see e.g., Sial et al., 2016; Grasby et al., 2019). Hg anomalies can be associated also with increased organic matter burial, as well as connected with Hg trapped by pyrite as a result of local redox variations and/or terrestrial input (e.g., Grasby et al., 2019; Shen et al., 2019). However, Hg content is correlated neither with TOC ($r = 0.15$; $p > 0.05$), nor TS content ($r = -0.07$; $p > 0.05$) in the Polanówka UW-1 core and both relationships are insignificant ($p > 0.05$). In the Stevns-1 core Hg vs. TOC correlation is generally low and insignificant ($r = 0.4$; $p > 0.05$) and that between Hg and TS is moderate and insignificant ($r = 0.55$; $p > 0.05$). This excludes the organic matter and sulphide fraction as major carriers of mercury, confirming that Hg enrichments are likely connected with an increased volcanic activity during the MME. The insignificant variation in the content and mineral composition of siliciclastic detritus in both sections can neither account for the observed Hg spikes.

The magnitude of the Hg anomalies observed across the MME in both cores is similar to those described from the limy Cretaceous–Paleogene boundary interval of the Bidart section in France (with a maximum of 46.6 ppb; (Font et al., 2016) and approximately half of those reported in the marls of the Elles section, Tunisia and Hor Hahar section, Israel (Keller et al., 2020), all of which reflect Deccan Traps volcanic activity. Comparable sizes of Hg anomalies (18 ppb with background level <6 ppb) are reported from carbonate-dominated Middle Permian successions in the Canadian Arctic, supposedly related to the eruption of the Emeishan flood basalts (Bond et al., 2020). Wedepohl and Merian (1991) estimated that Phanerozoic Hg concentrations in limestone reached on average 30 ppb. In contrast, Sial et al. (2010) documented background Hg levels in Precambrian, Mesozoic and Cenozoic carbonates from South America between 1.5 and 10 ppb, similar to the background levels observed in the Middle Permian of the Canadian Arctic or in the late Maastrichtian of Bidart. However, it has also been shown that Hg background levels in Phanerozoic carbonates can reach as high as >100 ppb while short-lived anomalies reach >1000 ppb (see e.g., Piszarska et al., 2020; R (Racki, 2020b)). Therefore, it seems more reasonable to compare Hg anomalies to the local sedimentary background level than to analyse the absolute values of Hg spikes. The magnitude of Hg spikes depends most probably on the proximity of magmatic centres and sources of mercury. For example, during the Mississippian anoxic event, the lower values of Hg enrichments in the Montagne Noire and Holy Cross Mts. regions imply that these sites were located farther from the active volcanic centers that were the sources of Hg to seawater and sediments. The highest values of Hg anomaly (<3650 ppb) in the Carnic Alps suggest that this area

was situated definitely closer to the active zone connected with the collision of the *peri-Gondwanan* Palaeo-Adria terranes (e.g., Rakociński et al., 2022, 2023).

5.2. Changes in seawater circulation in the European shelf Basin

The gradual trend towards less radiogenic $\epsilon_{\text{Nd}(t)}$ signature (i.e., lower $\epsilon_{\text{Nd}(t)}$ values) in intervals I-IV can be interpreted as an effect of either increased continental runoff or transient modification of water circulation with gradually increasing supply of water masses having less radiogenic Nd composition. Since the terrigenous flux did not fluctuate much in Polanówka UW-1 and the Nd isotope analysis was carried out on very well-preserved carbonate sedimentary material, the observed temporal trends in our $\epsilon_{\text{Nd}(t)}$ data should be interpreted with regard to changing water circulation. The only oceanic water masses capable of driving the seawater $\epsilon_{\text{Nd}(t)}$ in the Maastrichtian European epicontinental basin to lower values could be derived from the North Atlantic (MacLeod et al., 2011; Martin et al., 2012) and Boreal realms (Puceat et al., 2005), where continental runoff from weathering and erosion of Precambrian shields contributed to the unradiogenic Nd isotope signature of local seawater. Conversely, Pacific and Eastern or Southern Tethyan sources with relatively high $\epsilon_{\text{Nd}(t)}$ signatures (Stille et al., 1996; Puceat et al., 2005; Soudry et al., 2006; Martin et al., 2012) are excluded. Boreal provenance is unlikely, as the ingression of cold subarctic water masses would have caused water cooling and an increase in foraminiferal $\delta^{18}\text{O}$, which is not observed in the sections examined. Therefore, the most probable cause for the decline of $\epsilon_{\text{Nd}(t)}$ observed in intervals I-IV is an ingression of relatively unradiogenic North Atlantic water masses into the Chalk Sea around ~69 Ma (Martin et al., 2012). The relatively elevated $\epsilon_{\text{Nd}(t)}$ values observed in intervals I-II can be related to an increased flux of radiogenic Nd from a LIP, such as the Kerguelen hotspot, which is superimposed on the general trend related to changing ocean circulation. The evidence of this is the coincidence of the highest $\epsilon_{\text{Nd}(t)}$ values and the most prominent Hg/TOC peaks at 90.15 m, 88 m and 83.65 m in Polanówka UW-1.

Modification of ocean circulation patterns and the increasing contribution of North Atlantic water masses to the Chalk Sea are additionally supported by the appearance of complex heterohellicids *Planoglobulina* (*Planoglobulina brazoensis* and *P. carseyae*) in Polanówka UW-1 (Fig. 4. F, blue triangles). Ocean currents have a great impact on marine biota (Hays, 2017) including planktonic foraminifera (Nyong, 1984) for which peculiar changes in oceanic circulation can lead to colonization of new areas or, on the contrary, restriction of their biogeographical range. Therefore, fossil foraminiferal composition and distribution are important indicators of oceanic circulation changes. Complex heterohellicids are extremely rare in the Cretaceous European shelf seas. They were observed in the Central European Basin only in the studied MME-related interval (see Peryt et al., 2022). These taxa are in general frequent in the Tethyan Bioprovince and rare in Transitional provinces (Nederbragt, 1992), suggesting their migration from the Tethys. Nederbragt (1989) observed a *Planoglobulina* bloom during the middle Maastrichtian (the lowest part of the *A. mayorensis* Zone) in the northwestern Atlantic. This taxon likely migrated by following warm water current from the tropics to the North Atlantic and then further colonized the European shelf sea. Changes in global deep-ocean circulation during the mid-Maastrichtian have already been documented in the tropical Pacific, South Atlantic, Southern Ocean, and proto-Indian Ocean (Frank and Arthur, 1999; Jung et al., 2013; Voigt et al., 2013). However, due to the lack of clear geochemical proxies that can trace surface currents, no account has been provided so far of how deep-ocean reorganization could have possibly affected the intensity and/or direction of surface currents. We believe that planktic assemblages can actually

play this role via changes in their paleobiogeographic distributions and documentation of colonization events in distinct oceanic basins (see also Huber et al., 1992 and Thibault et al., 2010). Here, we suggest that the colonization of North Atlantic and Epicontinental Chalk Sea by large heterohellicids in the middle Maastrichtian reflects such changes in surface currents, perhaps via the birth and/or intensification of a proto-Gulf-stream. Previous studies have suggested the existence of a vigorous Gulf Stream already in the Maastrichtian (Watkins and Self-Trail, 2005; Thibault and Husson, 2016). The northwestern flow of warm waters from the Atlantic into the epicontinental Chalk Sea was also likely facilitated by the global eustatic sea-level rise that allowed for opening of new oceanic gateways.

Because osmium has a moderate oceanic residence time of ~10–30 kyr (Georg et al., 2013), which is longer than the ocean mixing time of ~1.5 kyr (Tachikawa et al., 2017), $^{187}\text{Os}/^{188}\text{Os}$ in open oceanic settings is globally uniform (Peucker-Ehrenbrink and Ravizza, 2000). However, local variations decoupled from the oceanic signature occur in restricted seas, where abundant continental runoff is able to alter the $^{187}\text{Os}/^{188}\text{Os}$ values of local seawater (Paquay and Ravizza, 2012). The direction of this modification depends on the source rocks in the catchment area, with relatively ^{187}Os -enriched sedimentary and felsic crystalline rocks and relatively ^{187}Os -depleted mantle-derived sources (Peucker-Ehrenbrink and Ravizza, 2000). The $^{187}\text{Os}/^{188}\text{Os}$ values at Polanówka UW-1 are relatively radiogenic and by <0.5 higher than those of coeval seawater of ~0.55–0.65 (Ravizza, 2007), which indicates decoupling of the local water column from oceanic water masses and influence of radiogenic continental runoff, in line with the position of this section in an epeiric basin (Du Vivier et al., 2014), and confirmed by the relatively high terrigenous detritus content at Polanówka UW-1. Precambrian shields and products of their weathering are especially important sources of radiogenic Os (Peucker-Ehrenbrink and Blum, 1998) and such rocks were cropping out on the surrounding European continent in the Late Cretaceous. However, organic carbon-rich sediments are also important sources of radiogenic Os, which is preferentially bound in labile organic matter that is easily decomposed in the presence of O_2 (Jaffe et al., 2002). We propose that the positive $^{187}\text{Os}/^{188}\text{Os}$ excursion observed in intervals I-II was driven by a rapid and widespread transgression onto weathered, soil-covered land rich in organic matter, and/or outcropping organic-rich sedimentary rocks. This transgression might have caused leaching of labile organic matter from extensive continental areas covered with weathered sediments, providing a sudden extra delivery of radiogenic Os to the epeiric sea. This effect was not, however, related to increased particulate riverine runoff, since the acceleration of terrigenous supply was not observed in the section. Peucker-Ehrenbrink and Blum (1998) suggested that elevated rate of radiogenic Os delivery to oceans takes place in the early stages of transgression following deglaciation, which increases the global oceanic $^{187}\text{Os}/^{188}\text{Os}$ budget. This scenario may be specifically linked to glacial production of large quantities of finely ground sediments enriched in radiogenic Os, which is preferentially released and transported to the oceans during postglacial humid periods with increased rates of chemical weathering (Derry, 2009). Reusch et al. (1998) reported on high-resolution oscillations in the mid-Miocene marine Os isotope record, which they linked to glacioeustatic fluctuations and increased weathering of exposed highly radiogenic continental materials during wet deglacial periods. We believe that a similar surplus radiogenic Os supply could have occurred during the onset of the MME (intervals I-II) under greenhouse conditions favouring intensive chemical weathering and pedogenesis. Continental input must have overshadowed the supply of unradiogenic Os from the LIP, as the average hydrothermal

Os flux is notoriously less significant than the continental Os flux (Peucker-Ehrenbrink and Ravizza, 2000).

Further confirmation of this scenario comes from the C/N ratio and other isotopic proxies coinciding with the positive $^{187}\text{Os}/^{188}\text{Os}$ excursion in intervals I–II. The C/N ratio is distinctively higher in these intervals, attesting of an increased contribution of organic matter from the land (Lamb et al., 2006). Elevated $\delta^{15}\text{N}_{\text{org}}$ values $>5\text{‰}$ in interval I match those in shelf sediments of shallow, oligotrophic seas, where riverine input is significant and ^{15}N -enriched dissolved organic nitrogen is the main nitrogen source (Gaye et al., 2009; Knapp et al., 2011). By analogy to modern shallow oligotrophic seas, where the $\delta^{15}\text{N}_{\text{org}}$ values decrease with depth (Knapp et al., 2011) and with distance from riverine source of ^{15}N -enriched nitrate (Mayer et al., 2002; Voss et al., 2006), the gradual decrease of $\delta^{15}\text{N}_{\text{org}}$ values in interval II is interpreted to have resulted from a shift to a deeper and more distal setting during the progressive sea-level rise. Still, all obtained values, $>3\text{‰}$, are higher than those in the open ocean areas dominated by N_2 fixation (Junium and Arthur, 2007), hence supporting the general influence of a ^{15}N -enriched continental runoff. The $\delta^{34}\text{S}_{\text{CAS}}$ values are generally close to the Maastrichtian seawater signature of 17–21‰ (Kampschulte and Strauss, 2004; Paytan et al., 2012). Relatively depleted values (16.7–19.0‰) are observed only in intervals I–III, and this may be related to an influence of land-derived flux of dissolved sulfate that is characterized by low $\delta^{34}\text{S}$ values (Bottrell and Newton, 2006), between 3 and 8‰ (Canfield, 2013) or even $<0\text{‰}$ (Claypool et al., 1980). The rise of foraminiferal $\delta^{13}\text{C}$ observed in interval I in both sections can also be interpreted as a result of rapid sea-level rise and associated transgression causing reworking of organic carbon-rich sediments and soils on previous land areas, causing enhanced nutrient levels in the epicontinental seas. Such circumstances could have promoted short-lived increased productivity and enhanced organic carbon burial rates leading to ^{13}C enrichment in the remaining marine dissolved inorganic carbon (DIC) pool (Jarvis et al., 2002).

After the short, but intensive transgressive pulse associated with an enhanced terrestrial influence recorded in the basal intervals I–III, vigorous ocean mixing occurred during the sea-level rise recorded in intervals III–IV. The $\varepsilon_{\text{Nd}(t)}$ values keep decreasing to approach those of the North Atlantic signature <-12 in these intervals, while the $^{187}\text{Os}/^{188}\text{Os}$ values reach their lowest level <0.8 , being very close to the open marine signature of ~ 0.6 (Ravizza, 2007). The $\delta^{15}\text{N}_{\text{org}}$ values stabilize at $\sim 4\text{‰}$, and the $\delta^{34}\text{S}_{\text{CAS}}$ values rise back to typical seawater signature of $\sim 20\text{‰}$. At the transition to interval V (74 m), the $\varepsilon_{\text{Nd}(t)}$ values rise by 1 ε unit and remain rather stable and low upsection (between -12.1 and -11.2), followed by a weak decreasing trend towards the top of the section. This insignificant $\varepsilon_{\text{Nd}(t)}$ variation in interval V does not allow to interpret the data in terms of ocean circulation. Similarly, C/N, $^{187}\text{Os}/^{188}\text{Os}$, and $\delta^{15}\text{N}_{\text{org}}$ remain at low levels in interval V, whereas the $\delta^{34}\text{S}_{\text{CAS}}$ values remain at the seawater level. These characteristics indicate that the basin was still influenced by continental runoff, but not as much as at the onset of the MME, because land-derived organic matter and leachable sources of Os, N, and S became strongly depleted during the initial phase of the transgression.

5.3. Foraminiferal $\delta^{18}\text{O}$ curves: temperature changes vs foraminiferal microhabitat effect

The three studied foraminiferal species, the epifaunal *Cibicides voltzianus*, infaunal *Gyroidinoides globosus* and planktonic planispiral *Planohedbergella prairiehillensis*, should record the $\delta^{18}\text{O}$ signature of their specific habitat in the seawater column, assuming no isotopic offset related to vital effect and provided that their shells are not diagenetically altered. In general, planktonic forami-

nifera are smaller and with much thinner test wall in comparison to benthic ones, so the isotope signatures archived in the planktic shells are more vulnerable to post-depositional changes. Therefore, only exquisitely preserved planktonic foraminifera should be considered as a reliable oceanographic geochemical information source (see Wendler et al., 2013). Due to the excellent preservation state of foraminiferal shell material in Polanówka UW-1 (see Fig. 5, Supplementary Table 2), diagenetic alteration appears unlikely. Preservation is not as good in the Stevns-1 material, compared to Polanówka. Nevertheless, the comparable $\delta^{18}\text{O}$ values of *P. prairiehillensis* in Polanówka UW-1 and Stevns-1, in the range of -1.3 to -0.8‰ and -1.5 to -0.8‰ , respectively (the $\delta^{18}\text{O}$ difference is only 0.1‰ on average, Fig. 3F1, 3F2, Supplementary Table 3), suggest that the original isotope signature has been preserved in both sections.

Most of recent planktonic foraminiferal species occur in greatest abundance within the upper 30–150 m of the water column (Rebotim et al., 2017; Tapia et al., 2022). Some species are more widespread in their average depth zones, whereas others show more restricted range. Surface dwellers show narrow average living depth ranges, being consistently concentrated in the surface layer $<50\text{ m}$ (Rebotim et al., 2017). The studied species *G. prairiehillensis* is a Cretaceous representative of surface-dwelling forms (e.g., Leckie, 1987), so we assume that even when including the seasonal vertical migration of the species, the average water depth range was rather narrow and located above the thermocline. Therefore, rather invariable $\delta^{18}\text{O}$ curves for planktonic foraminifera of the two localities (intervals I–V), suggest that both surface water temperature and DIC concentration (see Spero et al., 1997) were apparently stable during the studied intervals. Both factors are strongly interrelated by the fact that seawater absorbs the climate-driven CO_2 from the atmosphere (Mayot et al., 2023).

The difference in $\delta^{18}\text{O}$ values between planktonic and epifaunal benthic foraminifera is by $\sim 0.2\text{‰}$ larger in Polanówka ($\sim 0.5\text{‰}$) than in Stevns-1 ($\sim 0.3\text{‰}$), which is chiefly related to overall higher $\delta^{18}\text{O}$ values of the epibenthic *Cibicidoides* in Polanówka (average -0.5‰) than those in Stevns-1 (average -0.8‰ for interval x; Figs. 2, 3). The generally slightly lower $\delta^{18}\text{O}$ values for planktonic than epibenthic foraminifera are most probably related to water-column temperature gradients. Epibenthic foraminiferal shells are considered a reliable archive of bottom water isotope composition and an excellent proxy of long-term changes in deep-sea temperatures (Westerhold et al., 2020). Therefore, the average difference of $\sim 0.3\text{‰}$ (interval x in the Figs. 3, 4) in $\delta^{18}\text{O}$ values of epifaunal *Cibicidoides* between Polanówka UW-1 and Stevns-1 might be related to either slightly warmer and/or shallower bottom waters or, alternatively, to a higher amount of DIC in the Danish Basin (see Spero et al., 1997). A higher amount of DIC in the Danish Basin could be the result of a higher input of terrestrial organic matter and nutrients from the Fennoscandian Shield as compared to the Polish Basin (Fig. 1). Seawater DIC can potentially influence the $\delta^{18}\text{O}$ values of foraminifera by increasing the share of metabolic DIC for CaCO_3 production and therefore enhancing metabolic offsets (vital effect).

The longer-term trends in the $\delta^{18}\text{O}$ curves in Polanówka UW-1 for both epifaunal and infaunal foraminifera show a positive excursion from the base to $\sim 83\text{ m}$ with an amplitude of ~ 0.3 – 0.4‰ followed by a decreasing trend to $\sim 67\text{ m}$ with an amplitude of $\sim 0.6\text{‰}$ that might reflect a general cooling-warming trend in bottom waters. The long-term warming episode of the mid-Maastrichtian (between 69.5 and 67.5 Ma) in the Central European Shelf Basin has been documented by changes in bulk rock $\delta^{18}\text{O}$ and a nannofossil temperature index by Thibault et al., 2016. The positive shift in $\delta^{18}\text{O}$ for both benthic foraminiferal species at the bottom of the studied sections (intervals I and lowermost II) might reflect a short-lived cooling episode superimposed on this long-

term warming. A more pronounced warming of bottom waters in intervals II–V is in line with a change in ocean circulation and inflow of North Atlantic bottom water masses from low latitudes, as documented by our Nd isotope data. Such temperature trends are, however, not depicted in planktonic foraminifer O isotope curves, which suggests that the surface water temperature or amount of CO₂ were apparently more stable during the event.

On the other hand, warming-cooling trends in $\delta^{18}\text{O}$ curves in Polanówka for the two benthic species might be partially masked by changing the amount of DIC in the sediments and at the sediment–water interface. As already mentioned above, lower amounts of organic matter cause lower amounts of DIC available for calcification. The carbonate ion concentration ($[\text{CO}_3^{2-}]$) controls $\delta^{18}\text{O}$ in calcifying foraminifera (Spero et al., 1997), so that the $\delta^{18}\text{O}$ of calcite shells decreases with increasing concentration of DIC. In seawater, DIC is the limiting compound for CaCO₃ precipitation and requires an additional source. In marine organisms, DIC used for biocalcification is supplied from both metabolic CO₂ of organisms, seawater, and endosymbionts in photic zones (Sikes et al., 1981; Hu et al., 2020; Dubicka et al., 2023). In the late Cretaceous European shelf, marine ecosystems were largely controlled by their distance to the shoreline and nutrient delivery was influenced by this distance as well as water depth and sea-floor topography. For instance, the Cretaceous peak-transgression during latest Cenomanian and Turonian triggered highly oligotrophic blue-water systems on the European shelf from England to Russia (Gale et al., 2000; Linnert et al., 2010; Wiese et al., 2015; 2018). Accordingly, decreasing rates of particulate organic matter (POM) sink during sea-level rise (intervals II–IV) might have caused increasing $\delta^{18}\text{O}$ values of especially shallow infaunal *Gyroidinoides* that calcified within the sediment, in the top 2 cm (Corliss, 1991). Significant average difference in $\delta^{18}\text{O}$ values of $\sim 0.7\text{‰}$ between *Gyroidinoides* from Planówka and Stevns-1 might be similarly related to a more proximal location of Stevns-1 that was situated only ~ 200 km south of the emerged Fennoscandian Shield (Fig. 1).

Superimposed on these $\delta^{18}\text{O}$ long-term trends, a number of higher-frequency $\delta^{18}\text{O}$ variations appear particularly prominent for the infaunal foraminifera in intervals II–IV. Three positive peaks with amplitudes of $<0.4\text{‰}$ (peaks a–c) can be explained by short-term episodes of decreased DIC concentration (see above and Spero et al., 1997), which coincide and were probably linked to the severe oligotrophic conditions indicated by foraminiferal assemblages and their $\delta^{13}\text{C}$ values in intervals II–IV (see chapter 4.3). These oligotrophic episodes resulting in decreased DIC concentration possibly resulted in the *Stensioeina* extinction that is recorded within $\delta^{13}\text{C}$ peak c (Fig. 4). *Stensioeina* was one of the most abundant Cretaceous epifaunal foraminiferal taxa (Dubicka et al., 2014) that successively evolved since the latest Turonian within the European shelf seas. Before its extinction, *Stensioeina* constituted up to 33 % and 29 % of epibenthic foraminifera in Polanówka and Stevns-1, respectively, and was represented by at least three species. The *Stensioeina* disappearance is observed not only in the Polish and Danish basins but throughout NW Europe including the Maastrichtian type-area (Fig. 6F), where it also correlates with the extinction of ‘true inoceramids’ (Robaszynski et al., 1985).

5.4. Fluctuations in primary productivity

The increased $\delta^{18}\text{O}$ values of benthic foraminifera in intervals II–IV are associated with a general positive shift in the $\delta^{13}\text{C}$ of planktonic foraminifera in Polanówka likely reflecting a decreased rate of primary productivity in the water column (see Wendler et al., 2013). This part of the section is also characterized by an acme of coarse meridional ornamented *Rugoglobigerina*, a taxon linked with low-nutrient, oligotrophic environments, with a slow growth

rate and heavily calcified shells (Falzoni et al., 2014). The bloom of *Rugoglobigerina* and increase in planktonic $\delta^{13}\text{C}$ values correlate with a minor decreasing trend in the $\delta^{13}\text{C}$ of epifaunal *Cibicidoides* and an increase in $\delta^{13}\text{C}$ values of the infaunal *Gyroidinoides*. The $\delta^{13}\text{C}$ curve of infaunal *Gyroidinoides* converges towards that of epibenthic *Cibicidoides* at the transition from interval I into II, so that the $\delta^{13}\text{C}$ curves for these taxa are very close to each other in intervals II and III. Then, these curves diverge in interval IV and remain relatively distant from each other in intervals V and VI. Differences in $\delta^{13}\text{C}$ between shallow infaunal and epifaunal benthic foraminifera vary proportionally to the organic matter flux rate and the $\delta^{13}\text{C}_{\text{DIC}}$ gradient (e.g., Grossman, 1987; McCorkle et al., 1990; Mackensen et al., 2003; Schmittner et al., 2017) in the sediment column (isotopic microhabitat effect, e.g., Grossman, 1984; Ishimura et al., 2012). Thus, the increased $\delta^{13}\text{C}$ values of infaunal foraminifera and the associated decreased difference from those of epifaunal ones could have been caused by decelerated decomposition of ¹²C-enriched organic matter, which increased the overall $\delta^{13}\text{C}$ values of dissolved inorganic carbon ($\delta^{13}\text{C}_{\text{DIC}}$) in the pore water.

Suspended POM pools that are composed of detritus, zoo- and phytoplankton or bacteria, fuel marine ecosystem, as they are primary components of the marine carbon cycle and a major carbon source in marine sediments (Hoogakker et al., 2022). Low concentration of organic matter within the sediment during a sea-level highstand and under oligotrophic conditions might have additionally caused migration of the infaunal *Gyroidinoides* within the sediment column. Microhabitat structure of deep-sea benthic foraminifera is the function of food availability and oxygen concentration at the sea floor (Jorissen et al., 1995). Foraminifera are able to change their microhabitat in response to changing biogeochemical conditions (Linke and Lutze, 1993). Most infaunal foraminifera are deposit feeders that consume organic detritus. In oligotrophic environments with a limited amount of food, foraminiferal populations mainly comprise epibenthic taxa (Jorissen et al., 1995; Van Der Zwaan et al., 1999). Accordingly, positive trend in the $\delta^{13}\text{C}$ curve of the shallow-infaunal *Gyroidinoides* can be explained by a limited amount of organic detritus within the sediments during intervals II and III, which likely forced vertical migration of *Gyroidinoides* to the niche occupied by *Cibicidoides*, i.e. close to the sediment–water interface. This interpretation is supported by the simultaneous significant reduction in the abundance of deep-infaunal foraminifera within the total benthic foraminiferal assemblage (Fig. 3I).

The C/N ratios and $\delta^{13}\text{C}_{\text{org}}$ values indicate a mixed origin of organic matter, partly land-derived (Lamb et al., 2006). The relatively higher C/N ratios in intervals I–III suggest a higher contribution of land-derived marine organic matter at the onset of the MME-related transgression. Given the absence of notable TOC fluctuations and increased oligotrophy in intervals II–III, this increase in relative content of land-derived vs. marine organic matter could be partly attributed to a decreased marine primary productivity in these intervals. However, for interval I, the elevated C/N ratio is unequivocally linked to an increased terrestrial supply of organic matter. The CaCO₃ content measured across the entire Polanówka UW-1 section does not fluctuate much ($\sim 87 \pm 1.8\%$), which indicates insignificant variability of the terrigenous flux. It is confirmed by XRD data (Table 1) from intervals I–II showing stable content of detrital quartz and clay minerals at $\sim 10\%$, which is rather high for chalk. For comparison, chalk in the basal part of Stevns-1 is much purer with the CaCO₃ content of $\sim 96 \pm 2.2\%$. Therefore, the land-derived detrital and organic supplies were quite significant and stable in Polanówka, except at the onset of the MME where they decreased (Table 1). Kaolinite content in Polanówka UW-1 is very low and its ratio to illite+smectite drops only insignificantly at the top of interval II. The supply of products of chemical weather-

ing in the source land area was apparently low and decreased during the onset of the event. However, given rather small differences in the clay mineral composition and the limited number of samples analysed, we consider this variation as insignificant. Increased nutrient export via runoff from land can only be confirmed for interval I. Nutrient availability dropped afterwards coinciding with a reduction in marine primary productivity. Thus, we suggest that the low rate of primary productivity in intervals II and III was related to transgression and a gradual decrease in nutrient supply from the land.

5.5. Mid-Maastrichtian oceanographic changes linked to an active phase of large igneous province (LIP)?

The mid-Maastrichtian climate warming event has been found coeval to volcanic activity on the Ninetyeast Ridge (Kerguelen hotspot) (Keller et al., 2016) and to volcanic rocks dated from ~69.5 Ma over the next 2 million years (see also Kim et al., 2022). The Ninetyeast Ridge is a ~5500 km long, submarine volcanic ridge located in the eastern Indian Ocean. This is the longest linear feature on Earth attributed to volcanism that was generated by a deep-seated Kerguelen mantle plume (Nobre Silva et al., 2013). The ridge is the main hotspot track that formed by rapid northward drift of the Indian Plate over the Kerguelen hot spot during the Late Cretaceous (Weis and Frey, 1991; Nobre Silva et al., 2013). Ninetyeast Oceanic Ridge volcanism, which preceded or possibly co-existed with the first phase of Deccan eruptions (Keller et al., 2016), might have at least contributed to the temperature rise via associated atmospheric CO₂ emissions leading to a runaway greenhouse effect (see Kerr, 2005). Additional amounts of CO₂ might have been generated by contact metamorphism around intrusions within organic-rich sediments (Ernst and Youbi, 2017). Oceanic plateau formation could well explain the coincidence of a climate warming episode together with significant sea-level rise that might have been caused by the eruption of an enormous volume of lavas (~10×10⁶ km³) as well as by plume uplift of the ocean floor. In consequence, oceanic circulation system could have been modified significantly during the mid-Maastrichtian by opening of new water circulation pathways during sea-level rise as well as by shaping oceanic basin geometry by the appearance of large areas of uplifted sea-floor governing the course of the deep-oceanic water masses (see Kerr, 2005) and reinforcing deep-water convection (see Jung et al., 2013). Nowadays, the Kerguelen plateau plays a significant role in the global ocean's deep overturning circulation (Fukamachi et al., 2010).

The active phase of Kerguelen LIP could have triggered the sharp decrease in carbonate δ¹³C (MME2) by emission of greenhouse-gases. The long-term trend positive C isotope excursion that represents the overall MME may be linked to the sea-level rise and associated transgression, which enhanced burial of the ¹³C-depleted organic matter (see Jarvis et al., 2002), during a global warming episode while the short-lived MME2 negative anomaly remains enigmatic but could tentatively be explained by increased continental weathering caused by abnormally high temperature and atmospheric CO₂ level, increased rate of gas hydrate dissociation related to elevated temperature, and/or release of a significant amount of ¹²C from organic-rich sedimentary rocks heated by an intrusive component of a LIP. Moreover, we note that the first, more prominent positive excursion (MME-1 CIE) coincides with Hg anomalies in both sections, which we interpret as an effect of the emplacement of the Kerguelen LIP.

Along with sea-level rise, disruption of oceanic circulation patterns and the carbon cycle, possible oceanic acidification, toxic metal input including mercury poisoning, and other common LIP-related environmental stress factors could have triggered the biotic extinction (see Ernst and Youbi, 2017; Racki et al., 2018b;

Rakociński et al., 2021) including the demise of rudist reef ecosystems. Rudists were predominantly stenothermal and stenohaline occupying a shallow marine habitat in tropical zones (Jones and Nicol, 1986). As they possessed photosymbionts, which apparently enhanced their calcification process, they must have occupied marine photic settings (De Winter et al., 2020). We suggest here that the sudden and significant global transgression during the middle Maastrichtian might have been one of the causes for rudist-reef extinction, as their shallow-water tropical biotopes underwent a very rapid deepening. However, a more comprehensive and systematic research needs to be conducted in order to understand this relationship in detail. Because the MME-related interval is associated with abrupt global warming, rudists collapse in response to thermal stress is also of interest for future studies, in particular because temperature change is the main cause of today's coral crisis (e.g., Heron et al., 2016; Hughes et al., 2017). Modern corals live in a symbiotic relationship with microscopic algae (*Symbiodinium* spp.), that inhabit the body of corals, provide corals with up to 90 % of their energy (Heron et al., 2016), and possibly enhance the calcification process (Dubicka et al., 2023). However, during an increase in marine water temperature, when corals are stressed, they expel these algae, a process that is known as coral bleaching, which eventually leads to their death (e.g., Heron et al., 2016; Hughes et al., 2017).

6. Conclusions

The mid-Maastrichtian Event (MME) lasted ~2 Myr, spanning C31r and C30n magnetostratigraphic polarity zones, and was associated with a significant sea-level rise of ~50–100 m, with a long-term positive carbon isotope excursion interrupted by an abrupt, short-term negative shift. Anomalously high mercury concentrations recorded at that time in the Danish and Polish basins attest of volcanic–tectonic drivers, apparently LIP-related, which resulted in the global oceanographic perturbations in the mid-Maastrichtian. Production of vast oceanic plateaus, most probably linked to the Kerguelen hotspot, explains well the globally synchronous (1) climate warming likely caused by emission of greenhouse gases, (2) modification of the oceanic circulation system reinforcing deep-water convection due to sea-level rise and changes of ocean basin geometries, (3) disruption in the global carbon cycle, (4) biotic extinctions as a consequence of environmental stress caused by all these factors and/or additional LIP-related environmental impacts such as oceanic acidification or toxic metal input. MME-related changes also left their imprint upon the Epicontinental European Sea ecosystem where a number of oceanographic disturbances, such as changes in trophic structure, sea-water circulation, as well as biota migration and extinctions, have been recorded.

Author contributions

Z.D. and M.B. conceived the idea of the study and designed the study; WW and MJB performed lab work preceding geochemical studies; WW performed foraminiferal analysis including sample preparation, taxa designations and calculations. WW prepared the figures. MR provided Hg content data. ZD and MJB wrote the manuscript with contributions from all authors.

Declaration of Competing Interest

The authors declare that they have no known competing financial interests or personal relationships that could have appeared to influence the work reported in this paper.

Acknowledgments

The study was funded by the National Science Centre, Poland, grant no. 2017/27/B/ST10/00687. We are grateful to Michael Brauns (Mannheim, Germany) for Os isotope measurements and the description of methodology. We are also grateful to Zdzisław Bełka (Poznań, Poland) for Nd isotope measurements and the description of methodology.

Appendix A. Supplementary material

Supplementary data to this article can be found online at <https://doi.org/10.1016/j.gr.2023.11.010>.

References

- Barbin, V., 2013. Application of cathodoluminescence microscopy to recent and past biological materials: a decade of progress. *Mineralogy and Petrology* 107, 353–362. <https://doi.org/10.1007/s00710-013-0266-6>.
- Barral, A., Gomez, B., Fourel, F., Daviero-Gomez, V., Lécuyer, C., 2017. CO₂ and temperature decoupling at the million-year scale during the Cretaceous Greenhouse. *Scientific Reports* 7, <https://doi.org/10.1038/s41598-017-08234-0> 8310.
- Barrera, E., 1994. Global environmental changes preceding the Cretaceous-Tertiary boundary: Early-late Maastrichtian transition. *Geology* 22, [https://doi.org/10.1130/0091-7613\(1994\)022<0877:GECPTC>2.3.CO;2](https://doi.org/10.1130/0091-7613(1994)022<0877:GECPTC>2.3.CO;2) 877.
- Barrera, E., Savin, S.M., 1999. Evolution of late Campanian-Maastrichtian marine climates and oceans. In: Barrera, E., Johnson, C.C. (Eds.), *Evolution of the Cretaceous Ocean-Climate System*, Geological Society of America Special Paper 332, 245–282. [10.1130/0-8137-2332-9.245](https://doi.org/10.1130/0-8137-2332-9.245).
- Barrera, E., Savin, S.M., Thomas, E., Jones, C.E., 1997. Evidence for thermohaline-circulation reversals controlled by sea-level change in the latest Cretaceous. *Geology* 25, 715–718.
- Becker, M., Waksmundzka, K., Wójcik, K. (Eds.), 2023. *Maciejowice IG1. Profile Głębokich Otworów Wiertniczych*. Polish Geological Institute 167 ISBN: 978-83-67969-38-3 [In Polish]
- Birck, J.L., Barman, M.R., Capmas, F., 1997. Re-Os Isotopic Measurements at the Femtomole Level in Natural Samples. *Geostandards and Geoanalytical Research* 21, 19–27. <https://doi.org/10.1111/j.1751-908X.1997.tb00528.x>.
- Błaszkiwicz, A., 1980. *Campanian and Maastrichtian Ammonites of the Middle Vistula River Valley, Poland: a Stratigraphic-paleontological Study*. *Prace Instytutu Geologicznego* 92, 3–63.
- Bond, D.P.G., Wignall, P.B., Grasby, S.E., 2020. The Capitanian (Guadalupian, Middle Permian) mass extinction in NW Pangea (Borup Fiord, Arctic Canada): A global crisis driven by volcanism and anoxia. *Geological Society of America Bulletin* 132, 931–942. <https://doi.org/10.1130/B35281.1>.
- Bottrell, S.H., Newton, R.J., 2006. Reconstruction of changes in global sulfur cycling from marine sulfate isotopes. *Earth-Science Reviews* 75, 59–83. <https://doi.org/10.1016/j.earscirev.2005.10.004>.
- Boussaha, M., Thibault, N., Stemmerik, L., 2016. Integrated stratigraphy of the late Campanian-Maastrichtian in the Danish basin: revision of the Boreal calcareous nannofossil zonation. *Newsletters on Stratigraphy* 49, 337–360. <https://doi.org/10.1127/nos/2016/0075>.
- Bowman, V.C., Francis, J.E., Askin, R.A., Riding, J.B., Swindles, G.T., 2014. Latest Cretaceous–earliest Paleogene vegetation and climate change at the high southern latitudes: palynological evidence from Seymour Island, Antarctic Peninsula. *Palaeogeography, Palaeoclimatology, Palaeoecology* 408, 26–47. <https://doi.org/10.1016/j.palaeo.2014.04.018>.
- Brauns, C.M., 2001. A rapid, low-blank technique for the extraction of osmium from geological samples. *Chemical Geology* 176, 379–384. [https://doi.org/10.1016/S0009-2541\(00\)00371-5](https://doi.org/10.1016/S0009-2541(00)00371-5).
- Bromley, R.G., Ekdale, A.A., 1986. Composite ichnofabrics and tiering of burrows. *Geological Magazine* 123, 59–65. <https://doi.org/10.1017/S0016756800026534>.
- Brown, S.K., Croswell, H.S., Sparks, R.S.J., Cottrell, E., Deligne, N.I., Guerrero, N.O., Hobbs, L., Kiyosugi, K., Loughlin, S.C., Siebert, L., Takarada, S., 2014. Characterisation of the Quaternary eruption record: analysis of the Large Magnitude Explosive Volcanic Eruptions (LaMEVE) database. *Journal of Applied Volcanology* 3, 5. <https://doi.org/10.1186/2191-5040-3-5>.
- Bryan, S.E., Peate, I.U., Peate, D.W., Self, S., Jerram, D.A., Mawby, M.R., Marsh, J.S. (Goonie), Miller, J.A., 2010. The largest volcanic eruptions on Earth. *Earth-Science Reviews* 102, 207–229. [10.1016/j.earscirev.2010.07.001](https://doi.org/10.1016/j.earscirev.2010.07.001).
- Canfield, D.E., 2013. Sulfur isotopes in coal constrain the evolution of the Phanerozoic sulfur cycle. *Proceedings of the National Academy of Sciences U.S.A.* 110, 8443–8446. [10.1073/pnas.1306450110](https://doi.org/10.1073/pnas.1306450110).
- Caron, M., Homewood, P., 1983. Evolution of early planktic foraminifers. *Marine Micropaleontology* 7, 453–462. [https://doi.org/10.1016/0377-8398\(83\)90010-5](https://doi.org/10.1016/0377-8398(83)90010-5).
- Chauris, H., LeRousseau, J., Beaudoin, B., Propson, S., Montanari, A., 1998. Inoceramid extinction in the Gubbio basin (northeastern Apennines of Italy) and relations with mid-Maastrichtian environmental changes. *Palaeogeography, Palaeoclimatology, Palaeoecology* 139, 177–193. [https://doi.org/10.1016/S0031-0182\(97\)00150-8](https://doi.org/10.1016/S0031-0182(97)00150-8).
- Claypool, G.E., Holser, W.T., Kaplan, I.R., Sakai, H., Zak, I., 1980. The age curves of sulfur and oxygen isotopes in marine sulfate and their mutual interpretation. *Chemical Geology* 28, 199–260. [https://doi.org/10.1016/0009-2541\(80\)90047-9](https://doi.org/10.1016/0009-2541(80)90047-9).
- Cogné, J.-P., Humler, E., 2006. Trends and rhythms in global seafloor generation rate: seafloor generation rate. *Geochemistry, Geophysics, Geosystems* 7. <https://doi.org/10.1029/2005GC001148>.
- Conrad, C.P., 2013. The solid Earth's influence on sea level. *Geological Society of America Bulletin* 125, 1027–1052. <https://doi.org/10.1130/B30764.1>.
- Copper, P., 1994. Ancient reef ecosystem expansion and collapse. *Coral Reefs* 13, 3–11. <https://doi.org/10.1007/BF00426428>.
- Corliss, B.H., 1991. Morphology and microhabitat preferences of benthic foraminifera from the northwest Atlantic Ocean. *Marine Micropaleontology* 17, 195–236. [https://doi.org/10.1016/0377-8398\(91\)90014-W](https://doi.org/10.1016/0377-8398(91)90014-W).
- Corliss, B.H., Chen, C., 1988. Morphotype patterns of Norwegian Sea deep-sea benthic foraminifera and ecological implications. *Geology* 16, 716. [https://doi.org/10.1130/0091-7613\(1988\)016<0716:MPONSD>2.3.CO;2](https://doi.org/10.1130/0091-7613(1988)016<0716:MPONSD>2.3.CO;2).
- Cox, J.R., 1969. Inoceramidae. In: Moore, R.C. (Ed.), *Treatise on Invertebrate Paleontology, Part n, Volume 1, Mollusca 6, N314–N321*. Geological Society of America and The University of Kansas Press, Boulder and Lawrence, p. 1969.
- Crampton, J.S., 1988. Comparative taxonomy of the bivalve families Isognomonidae, Inoceramidae, and Retroceramidae. *Palaeontology* 31, 965–996.
- De Winter, N.J., Goderis, S., Van Malderen, S. J. M., Sinnesael, M., Vansteenberghe, S., Snoeck, C., Belza, J., Vanhaecke, F., Claeys, P., 2020. Subdaily-scale chemical variability in a Torretites Sanchezi rudist shell: implications for rudist paleobiology and the Cretaceous day-night cycle. *Paleoceanography and Paleoclimatology* 35, [e2019PA003723]. [10.1029/2019PA003723](https://doi.org/10.1029/2019PA003723).
- Derry, L.A., 2009. A glacial hangover. *Nature* 458, 417–418. <https://doi.org/10.1038/458417a>.
- Dopieralska, J., 2009. Reconstructing seawater circulation on the Moroccan shelf of Gondwana during the Late Devonian: Evidence from Nd isotope composition of conodonts: neodymium isotopes in Devonian conodonts. *Geochemistry, Geophysics, Geosystems* 10. <https://doi.org/10.1029/2008GC002247>.
- Du Vivier, A.D.C., Selby, D., Sageman, B.B., Jarvis, I., Gröcke, D.R., Voigt, S., 2014. Marine 187Os/188Os isotope stratigraphy reveals the interaction of volcanism and ocean circulation during Oceanic Anoxic Event 2. *Earth and Planetary Science Letters* 389, 23–33. <https://doi.org/10.1016/j.epsl.2013.12.024>.
- Dubicka, Z., 2019. Chamber arrangement versus wall structure in the high-rank phylogenetic classification of Foraminifera. *Acta Palaeontologica Polonica* 64 (1), 1–18. <https://doi.org/10.4202/app.00564.2018>.
- Dubicka, Z., Peryt, D., 2012a. Latest Campanian and Maastrichtian palaeoenvironmental changes: Implications from an epicontinental sea (SE Poland and western Ukraine). *Cretaceous Research* 37, 272–284. <https://doi.org/10.1016/j.cretres.2012.04.009>.
- Dubicka, Z., Peryt, D., 2012b. The Lower/Upper Maastrichtian boundary interval in the Lublin Syncline (SE Poland, Boreal realm): new insight into foraminiferal stratigraphy. *Newsletters on Stratigraphy* 45, 139–150. <https://doi.org/10.1127/0078-0421/2012/0018>.
- Dubicka, Z., Peryt, D., Szuszkiewicz, M., 2014. Foraminiferal evidence for paleogeographic and paleoenvironmental changes across the Coniacian-Santonian boundary in western Ukraine. *Palaeogeography Palaeoclimatology Palaeoecology* 401, 43–56. <https://doi.org/10.1016/j.palaeo.2014.03.002>.
- Dubicka, Z., Owocik, K., Gloc, M., 2018. Micro- and nanostructures of calcareous foraminiferal tests: insight from some representatives of Miliolida, Rotaliida and Lagenida. *Journal of Foraminiferal Research* 48, 142–155. <https://doi.org/10.2113/jsjfr.48.2.142>.
- Dubicka, Z., Wierzbowski, H., Wierny, W., 2018. Oxygen and carbon isotope records of Upper Cretaceous foraminifera from Poland: vital and microhabitat effects. *Palaeogeography, Palaeoclimatology, Palaeoecology* 500, 33–51. <https://doi.org/10.1016/j.palaeo.2018.03.029>.
- Dubicka, Z., Bojanowski, M.J., Bijma, J., Bickmeyer, U., 2023. Mg-rich amorphous to Mg-low crystalline CaCO₃ pathway in foraminifera. *Heliyon* 9, e18331.
- Ekdale, A.A., Bromley, R.G., 1984. Comparative Ichnology of Shelf-Sea and Deep-Sea Chalk. *Journal of Paleontology* 58, 322–332.
- Ekdale, A.A., Bromley, R.G., 1991. Analysis of Composite Ichnofabrics: An Example in Uppermost Cretaceous Chalk of Denmark. *Palaios* 6, 232–249. <https://doi.org/10.2307/3514904>.
- Eldholm, O., and M.F. Coffin., 2000. Large igneous provinces and plate tectonics. Pp. 309–326 in *The History and Dynamics of Global Plate Motions*, M.A. Richards, R. G. Gordon, and R.D. van der Hilst, eds. American Geophysical Union Geophysical Monograph 121. American Geophysical Union, Washington, D.C.
- Ernst, R.E., Youbi, N., 2017. How Large Igneous Provinces affect global climate, sometimes cause mass extinctions, and represent natural markers in the geological record. *Palaeogeography, Palaeoclimatology, Palaeoecology* 478, 30–52. <https://doi.org/10.1016/j.palaeo.2017.03.014>.
- Falzone, F., Petrizzo, M.R., Huber, B.T., MacLeod, K.G., 2014. Insights into the meridional ornamentation of the planktonic foraminiferal genus *Rugoglobigerina* (Late Cretaceous) and implications for taxonomy. *Cretaceous Research* 47, 87–104. <https://doi.org/10.1016/j.cretres.2013.11.001>.

- Fanton, K.C., Holmden, C., Nowlan, G.S., Haidl, F.M., 2002. ¹⁴³Nd/¹⁴⁴Nd and Sm/Nd stratigraphy of Upper Ordovician epeiric sea carbonates. *Geochimica Et Cosmochimica Acta* 66, 241–255. [https://doi.org/10.1016/S0016-7037\(01\)00773-6](https://doi.org/10.1016/S0016-7037(01)00773-6).
- Fischer, A.G., Bottjer, D.J., 1995. Oxygen-depleted waters: A lost biotope and its role in ammonite and bivalve evolution. *Neues Jahrbuch Für Geologie Und Paläontologie* 195, 133–146. <https://doi.org/10.1127/njgpa/195/1995/133>.
- Föllmi, K.B., 2012. Early Cretaceous life, climate and anoxia. *Cretaceous Research* 35, 230–257.
- Font, E., Adatte, T., Sial, A.N., Drude de Lacerda, L., Keller, G., Punejar, J., 2016. Mercury anomaly, Deccan volcanism, and the end-Cretaceous mass extinction. *Geology* 44, 171–174. <https://doi.org/10.1130/G37451.1>.
- Frank, T.D., Arthur, M.A., 1999. Tectonic forcings of Maastrichtian ocean-climate evolution. *Paleoceanography* 14, 103–117. <https://doi.org/10.1029/1998PA900017>.
- Frank, T.D., Thomas, D.J., Leckie, R.M., Arthur, M.A., Bown, P.R., Jones, K., Lees, J.A., 2005. The Maastrichtian record from Shatsky Rise (northwest Pacific): A tropical perspective on global ecological and oceanographic changes: Maastrichtian record at Shatsky Rise. *Paleoceanography* 20. <https://doi.org/10.1029/2004PA001052>.
- Friedrich, O., Herrle, J.O., Wilson, P.A., Cooper, M.J., Erbacher, J., Hemleben, C., 2009. Early Maastrichtian carbon cycle perturbation and cooling event: Implications from the South Atlantic Ocean: Maastrichtian isotope perturbations. *Paleoceanography* 24. <https://doi.org/10.1029/2008PA001654>.
- Fukamachi, Y., Rintoul, S.R., Church, J.A., Aoki, S., Sokolov, S., Rosenberg, M.A., Wakatsuchi, M., 2010. Strong export of Antarctic Bottom Water east of the Kerguelen plateau. *Nature Geoscience* 3, 327–331. <https://doi.org/10.1038/ngeo842>.
- Gale, A.S., Smith, A.B., Monks, N.E.A., Young, J.A., Howard, A., Wray, D.S., Huggett, J.M., 2000. Marine biodiversity through the Late Cenomanian–Early Turonian: palaeoceanographic controls and sequence stratigraphic biases. *Journal of the Geological Society* 157, 745–757. <https://doi.org/10.1144/jgs.157.4.745>.
- Gaye, B., Wiesner, M.G., Lahajnar, N., 2009. Nitrogen sources in the South China Sea, as discerned from stable nitrogen isotopic ratios in rivers, sinking particles, and sediments. *Marine Chemistry* 114, 72–85. <https://doi.org/10.1016/j.marchem.2009.04.003>.
- Georg, R.B., West, A.J., Vance, D., Newman, K., Halliday, A.N., 2013. Is the marine osmium isotope record a probe for CO₂ release from sedimentary rocks? *Earth and Planetary Science Letters* 367, 28–38. <https://doi.org/10.1016/j.epsl.2013.02.018>.
- Gómez-Alday, J.J., López, G., Elorza, J., 2004. Evidence of climatic cooling at the Early/Late Maastrichtian boundary from inoceramid distribution and isotopes: Sopolana sections, Basque Country, Spain. *Cretaceous Research* 25, 649–668. <https://doi.org/10.1016/j.cretres.2004.06.009>.
- Gómez-Alday, J.J., Cruz Zuluaga, M., Elorza, J., 2008. ⁸⁷Sr/⁸⁶Sr ratios in inoceramids (Bivalvia) and carbonate matrix as indicators of differential diagenesis during burial. Early Maastrichtian Bay of Biscay sections (Spain and France). Potential use for chemostratigraphy? *Cretaceous Research* 29, 563–576. <https://doi.org/10.1016/j.cretres.2008.01.008>.
- Grasby, S.E., Them, T.R., Chen, Z., Yin, R., Ardakani, O.H., 2019. Mercury as a proxy for volcanic emissions in the geologic record. *Earth-Science Reviews* 196. <https://doi.org/10.1016/j.earscirev.2019.102880>.
- Green, O.R., 2001. *A Manual of Practical Laboratory and Field Techniques in Palaeobiology*. Kluwer Academic, London, p. 538.
- Grossman, E.L., 1984. Stable isotope fractionation in live benthic foraminifera from the southern California Borderland. *Palaeogeography, Palaeoclimatology, Palaeoecology* 47, 301–327. [https://doi.org/10.1016/0031-0182\(84\)90100-7](https://doi.org/10.1016/0031-0182(84)90100-7).
- Grossman, E.L., 1987. Stable isotopes in modern benthic foraminifera: a study of vital effect. *Journal of Foraminiferal Research* 16, 48–61.
- Gurnis, M., 1990. Ridge spreading, subduction, and sealevel fluctuations. *Science* 250, 970–972. <https://doi.org/10.1126/science.250.4983.970>.
- Hancock, J.M., 1989. Sea-level changes in the British region during the Late Cretaceous. *Proceedings of the Geologists' Association* 100, 565–594.
- Hancock, J.M., 1993. Transatlantic correlations in the Campanian–Maastrichtian stages by eustatic changes of sea-level. *Geological Society London, Special Publications* 70, 241–256.
- Hancock, J.M., 1975. The sequence of facies in the Upper Cretaceous of northern Europe compared with that in the Western Interior. In: Caldwell, W.G.E. (Eds.), *The Cretaceous System in the Western Interior of North America*. Geological Association of Canada, Special Paper 13, 83–118.
- Harriss, P.J., Crampton, J.S., 1998. The Inoceramids. *American Paleontologist* 6, 2–6.
- Hart, M.B., Bailey, H.W., 1979. The distribution of planktonic Foraminifera in the mid-Cretaceous of NW Europe. In: Wiedmann, J. (Eds.), *Aspekte der Kriede Europas*. International Union of Geological Sciences Series A, 6, 527–542.
- Hays, G.C., 2017. Ocean currents and marine life. *Current Biology* 27, R470–R473. <https://doi.org/10.1016/j.cub.2017.01.044>.
- Heinberg, C., 1979. *Bivalves from the Falest Maaslichlian of Stevns Klint and Their Stratigraphic Affinities*. University of Copenhagen, Cretaceous-Tertiary Boundary Events Symposium, pp. 58–65.
- Heron, S.F., Maynard, J.A., Van Hooidonk, R., Eakin, C.M., 2016. Warming Trends and Bleaching Stress of the World's Coral Reefs 1985–2012. *Scientific Reports* 6. <https://doi.org/10.1038/srep38402>.
- Hoogakker, B.A.A., Anderson, C., Paoloni, T., Stott, A., Grant, H., Keenan, P., Mahaffey, C., Blackbird, S., McClymont, E.L., Rickaby, R., Poulton, A., Peck, V.L., 2022. Planktonic foraminifera organic carbon isotopes as archives of upper ocean carbon cycling. *Nature Communications* 13. <https://doi.org/10.1038/s41467-022-32480-0>.
- Hu, M.Y., Petersen, I., Chang, W.W., Blurton, C., Stumpp, M., 2020. Cellular bicarbonate accumulation and vesicular proton transport promote calcification in the sea urchin larva. *Proceedings of the Royal Society B: Biological Sciences* 287, 20201506. <https://doi.org/10.1098/rspb.2020.1506>.
- Huber, B.T., Watkins, D., 1992. Biogeography of Campanian–Maastrichtian calcareous plankton in the region of the Southern Ocean: Paleogeographic and paleoclimatic implications. In: Kennett, J.P., Warnke, D.A. (Eds.), *The Antarctic Paleoenvironment: a Perspective on Global Change*, Antarctic Research Series, Series 56. American Geophysical Union, Washington, D.C., pp. 31–60.
- Huber, B.T., Norris, R.D., MacLeod, K.G., 2002. Deep-sea paleotemperature record of extreme warmth during the Cretaceous. *Geology* 30. [https://doi.org/10.1130/0091-7613\(2002\)030<0123:DSPROE>2.0.CO;2](https://doi.org/10.1130/0091-7613(2002)030<0123:DSPROE>2.0.CO;2).
- Huber, B.T., Petrizzo, M.R., Falzoni, F., 2022. Taxonomy and phylogeny of Albian–Maastrichtian planispiral planktonic foraminifera traditionally assigned to *Globigerinelloides*. *Micropaleontology* 68, 117–183. <https://doi.org/10.47894/mpal.68.2.01>.
- Hughes, T.P., Kerry, J.T., Álvarez-Noriega, M., Álvarez-Romero, J.G., Anderson, K.D., Baird, A.H., Babcock, R.C., Beger, M., Bellwood, D.R., Berkelmans, R., Bridge, T.C., Butler, I.R., Byrne, M., Cantin, N.E., Comeau, S., Connolly, S.R., Cumming, G.S., Dalton, S.J., Diaz-Pulido, G., Eakin, C.M., Figueira, W.F., Gilmour, J.P., Harrison, H. B., Heron, S.F., Hoey, A.S., Hobbs, J.-P.-A., Hoogenboom, M.O., Kennedy, E.V., Kuo, C., Lough, J.M., Lowe, R.J., Liu, G., McCulloch, M.T., Malcolm, H.A., McWilliam, M. J., Pandolfi, J.M., Pears, R.J., Pratchett, M.S., Schoepf, V., Simpson, T., Skirving, W. J., Sommer, B., Torda, G., Wachenfeld, D.R., Willis, B.L., Wilson, S.K., 2017. Global warming and recurrent mass bleaching of corals. *Nature* 543, 373–377. <https://doi.org/10.1038/nature21707>.
- Isaza-Londoño, C., MacLeod, K.G., Huber, B.T., 2006. Maastrichtian North Atlantic warming, increasing stratification, and foraminiferal paleobiology at three timescales: North Atlantic Maastrichtian warming. *Paleoceanography* 21. <https://doi.org/10.1029/2004PA001130>.
- Isbell, J.L., Miller, M.F., Wolfe, K.L., Lenaker, P.A., 2003. Timing of late Paleozoic glaciation in Gondwana: Was glaciation responsible for the development of Northern Hemisphere cyclotherms? In: *Extreme Depositional Environments: Mega End Members in Geologic Time*. Geological Society of America, 10.1130/0-8137-2370-1-5.
- Ishimura, T., Tsunogai, U., Hasegawa, S., Nakagawa, F., Oi, T., Kitazato, H., Suga, H., Toyofuku, T., 2012. Variation in stable carbon and oxygen isotopes of individual benthic foraminifera: tracers for quantifying the magnitude of isotopic disequilibrium. *Biogeosciences* 9, 4353–4367. <https://doi.org/10.5194/bg-9-4353-2012>.
- Jackson, M.L., Barak, P.W., 2005. *Soil chemical analysis: advanced course: a manual of methods useful for instruction and research in soil chemistry, physical chemistry of soils, soil fertility, and soil genesis, Revised*. Parallel Press, University of Wisconsin-Madison Libraries, Madison, Wisconsin.
- Jacobsen, S.B., Wasserburg, G.J., 1980. Sm–Nd isotopic evolution of chondrites. *Earth and Planetary Science Letters* 50, 139–155. [https://doi.org/10.1016/0012-821X\(80\)90125-9](https://doi.org/10.1016/0012-821X(80)90125-9).
- Jaffe, L.A., Peucker-Ehrenbrink, B., Petsch, S.T., 2002. Mobility of rhenium, platinum group elements and organic carbon during black shale weathering. *Earth and Planetary Science Letters* 198, 339–353. [https://doi.org/10.1016/S0012-821X\(02\)00526-5](https://doi.org/10.1016/S0012-821X(02)00526-5).
- Jagt, J.W.M., Jagt-Yazykova, E.A., 2018. Stratigraphical ranges of tegulated inoceramid bivalves in the type area of the Maastrichtian Stage (Belgium, the Netherlands). *Cretaceous Research* 87, 385–394. <https://doi.org/10.1016/j.cretres.2017.05.022>.
- Jarvis, I., Mabrouk, A., Moody, R.T.J., De Cabrera, S., 2002. Late Cretaceous (Campanian) carbon isotope events, sea-level change and correlation of the Tethyan and Boreal realms. *Palaeogeography, Palaeoclimatology, Palaeoecology* 188, 215–248. [https://doi.org/10.1016/S0031-0182\(02\)00578-3](https://doi.org/10.1016/S0031-0182(02)00578-3).
- Johnson, C.C., 2002. The Rise and Fall of Rudist Reefs: Reefs of the dinosaur era were dominated not by corals but by odd mollusks, which died off at the end of the Cretaceous from causes yet to be discovered. *American Scientist* 90, 148–153.
- Johnson, C.C., Kauffman, E.G., 1990. Originations, radiations and extinctions of Cretaceous rudistid bivalve species in the Caribbean Province. In: Kauffman, E.G., Walliser, O.H. (Eds.), *Extinction Events in Earth History*, Lecture Notes in Earth Sciences. Springer-Verlag, Berlin/Heidelberg 305–324. [10.1007/BFb0011154](https://doi.org/10.1007/BFb0011154).
- Johnson, C.C., Kauffman, E.G., 1996. Maastrichtian extinction patterns of Caribbean Province rudistids. In: MacLeod, N., Keller, G. (Eds.), *The Cretaceous-Tertiary Mass Extinction: Biotic and Environmental Events*. New York, W.W. Norton and Co, pp. 231–273.
- Jones, D.S., Nicol, D., 1986. Origination, survivorship, and extinction of rudist taxa. *Journal of Paleontology* 60, 107–115. <https://doi.org/10.1017/S0022336000021557>.
- Jorissen, F.J., De Stigter, H.C., Widmark, J.G.V., 1995. A conceptual model explaining benthic foraminiferal microhabitats. *Marine Micropaleontology* 26, 3–15. [https://doi.org/10.1016/0377-8398\(95\)00047-X](https://doi.org/10.1016/0377-8398(95)00047-X).
- Jorissen, F.J., De Stigter, H.C., Widmark, J.G.V., 1995. A conceptual model explaining benthic foraminiferal microhabitats. *Marine Micropaleontology* 26, 3–15. [https://doi.org/10.1016/0377-8398\(95\)00047-X](https://doi.org/10.1016/0377-8398(95)00047-X).
- Jung, C., Voigt, S., Friedrich, O., Koch, M.C., Frank, M., 2013. Campanian–Maastrichtian ocean circulation in the tropical Pacific: Late Cretaceous ocean circulation. *Paleoceanography* 28, 562–573. <https://doi.org/10.1002/palo.20051>.

- Junium, C.K., Arthur, M.A., 2007. Nitrogen cycling during the Cretaceous, Cenomanian-Turonian Oceanic Anoxic Event II: Cretaceous nitrogen cycling. *Geochemistry, Geophysics, Geosystems* 8. <https://doi.org/10.1029/2006GC001328>.
- Kampschulte, A., Strauss, H., 2004. The sulfur isotopic evolution of Phanerozoic seawater based on the analysis of structurally substituted sulfate in carbonates. *Chemical Geology* 204, 255–286. <https://doi.org/10.1016/j.chemgeo.2003.11.013>.
- Kauffman, E.G., Sageman, B.B., Kirkland, J.L., Elder, W.P., Harries, P.J., Villamil, T., 1994. Molluscan biostratigraphy of the Cretaceous Western Interior Basin, North America. In: Caldwell, W.G.W., Kauffman, E.G. (Eds.), *Evolution of the Western Interior Basin*. Special Paper of the Geological Association of Canada 39, 397–434.
- Kauffman, E.G., Hart, M.B., 1996. *Cretaceous Bio-Events*. In: Walliser, O.H. (Ed.), *Events and Event Stratigraphy*. Springer-Verlag, Berlin.
- Kauffman, E.G., Johnson, C.C., 1988. The morphological and ecological evolution of middle and Upper Cretaceous reef-building rudistids. *Palaios* 3, 194–216.
- Kauffman, E.G., Runnegar, B., 1975. *Atomodesma* (Bivalvia), and Permian species of the United States. *Journal of Paleontology* 49, 23–51.
- Kauffman, E.G., 1975. Dispersal and biostratigraphic potential of Cretaceous benthonic bivalvia in the Western Interior. In: Caldwell, W.G.E. (Eds.), *The Cretaceous System in the Western Interior of North America*. The Geological Association of Canada Special Paper 13, 163–194.
- Keller, G., Punekar, J., Mateo, P., 2016. Upeavals during the late Maastrichtian: Volcanism, climate and faunal events preceding the end-Cretaceous mass extinction. *Palaeogeography, Palaeoclimatology, Palaeoecology* 441, 137–151. <https://doi.org/10.1016/j.palaeo.2015.06.034>.
- Keller, G., Mateo, P., Monkenbusch, J., Thibault, N., Punekar, J., Spangenberg, J.E., Abramovich, S., Aschkenazi-Polivoda, S., Schoene, B., Eddy, M.P., Samperton, K. M., Khadri, S.F.R., Adatte, T., 2020. Mercury linked to decan volcanism, climate change and the end-cretaceous mass extinction. *Global and Planetary Change* 194. <https://doi.org/10.1016/j.gloplacha.2020.103312> 103312.
- Kerr, A.C., 2005. Oceanic LIPs: the kiss of death. *Elements* 1, 289–292. <https://doi.org/10.1017/gselements.1.5.289>.
- Kerr, A.C., White, R.V., Saunders, A.D., 2000. LIP reading: recognizing oceanic plateaux in the geological record. *Journal of Petrology* 41, 1041–1056. <https://doi.org/10.1093/petrology/41.7.1041>.
- Keutgen, N., 2018. A bioclast-based astronomical timescale for the Maastrichtian in the type area (southeast Netherlands, northeast Belgium) and stratigraphic implications: the legacy of P.J. Felder. *Netherlands Journal of Geosciences* 97, 229–260. <https://doi.org/10.1017/njg.2018.15>.
- Kim, J.-E., Westerhold, T., Alegret, L., Drury, A.J., Röhl, U., Griffith, E.M., 2022. Precessional pacing of tropical ocean carbon export during the Late Cretaceous. *Climate of the past* 18, 2631–2641. <https://doi.org/10.5194/cp-18-2631-2022>.
- Knapp, A.N., Sigman, D.M., Lipschultz, F., Kustka, A.B., Capone, D.G., 2011. Interbasin isotopic correspondence between upper-ocean bulk DON and subsurface nitrate and its implications for marine nitrogen cycling: bulk marine DON $\delta^{15}N$. *Global Biogeochemical Cycles* 25 (4). <https://doi.org/10.1029/2010GB003878>.
- Kominz, M.A., Browning, J.V., Miller, K.G., Sugarman, P.J., Mizintseva, S., Scotese, C.R., 2008. Late Cretaceous to Miocene sea-level estimates from the New Jersey and Delaware coastal plain coreholes: an error analysis. *Basin Research* 20, 211–226. <https://doi.org/10.1111/j.1365-2117.2008.00354.x>.
- Kumar, A., 2019. Pollen-spore assemblages of the Navarro Group (Maastrichtian) of Texas, USA: biostratigraphical and palaeoecological significance. *Journal of Palaeosciences* 68, 147–162. <https://doi.org/10.54991/jop.2019.41>.
- Ladant, J.B., Donnadieu, Y., 2016. Palaeogeographic regulation of glacial events during the Cretaceous supergreenhouse. *Nature Communication* 7, 1277.
- Lamb, A.L., Wilson, G.P., Leng, M.J., 2006. A review of coastal palaeoclimate and relative sea-level reconstructions using $\delta^{13}C$ and C/N ratios in organic material. *Earth-Science Reviews* 75, 29–57. <https://doi.org/10.1016/j.earscirev.2005.10.003>.
- Larson, R.L., 1991. Latest pulse of Earth: Evidence for a mid-Cretaceous superplume. *Geology* 19. [https://doi.org/10.1130/0091-7613\(1991\)019<0547:LPOEEF>2.3.CO;2](https://doi.org/10.1130/0091-7613(1991)019<0547:LPOEEF>2.3.CO;2) 547.
- Leckie, R.M., 1987. Paleocology of mid-Cretaceous planktonic foraminifera: a comparison of open ocean and epicontinental sea assemblages. *Micropaleontology* 33. <https://doi.org/10.2307/1485491> 164.
- Li, L., Keller, G., 1998. Maastrichtian climate, productivity and faunal turnovers in planktic foraminifera in South Atlantic DSDP sites 525A and 21. *Marine Micropaleontology* 33, 55–86. [https://doi.org/10.1016/S0377-8398\(97\)00027-3](https://doi.org/10.1016/S0377-8398(97)00027-3).
- Li, L., Keller, G., 1999. Variability in Late Cretaceous climate and deep waters: evidence from stable isotopes. *Marine Geology* 161, 171–190.
- Linke, P., Lutze, G.F., 1993. Microhabitat preferences of benthic foraminifera: a static concept or a dynamic adaptation to optimize food acquisition? *Marine Micropaleontology* 20, 215–234. [https://doi.org/10.1016/0377-8398\(93\)90034-U](https://doi.org/10.1016/0377-8398(93)90034-U).
- Linnert, C., Mutterlose, J., Erbacher, J., 2010. Calcareous nannofossils of the Cenomanian/Turonian boundary interval from the Boreal Realm (Wunstorf, northwest Germany). *Marine Micropaleontology* 74, 38–58. <https://doi.org/10.1016/j.marmicro.2009.12.002>.
- Linnert, C., Robinson, S.A., Lees, J.A., Bown, P.R., Pérez-Rodríguez, I., Pettrizo, M.R., Falzoni, F., Littler, K., Arz, J.A., Russell, E.E., 2014. Evidence for global cooling in the Late Cretaceous. *Nature Communications* 5. <https://doi.org/10.1038/ncomms5194> 4194.
- Liu, L., Gurnis, M., Seton, M., Saleeby, J., Müller, R.D., Jackson, J.M., 2010. The role of oceanic plateau subduction in the Laramide orogeny. *Nature Geoscience* 3, 353–357. <https://doi.org/10.1038/ngeo829>.
- Machalski, M., 2005. Late Maastrichtian and earliest Danian ammonites from central Europe: taxonomy, evolution and extinction. *Acta Palaeontologica Polonica* 50, 653–696.
- Mackensen, A., Licari, L., 2003. Carbon isotopes of live benthic foraminifera from the South Atlantic: sensitivity to bottom water carbonate saturation state and organic matter rain rates. In: Wefer, G., Mulitza, S., Ratmeyer, V. (Eds.), *The South Atlantic in the Late Quaternary*. Springer, Berlin Heidelberg, Berlin, Heidelberg, pp. 623–644. https://doi.org/10.1007/978-3-642-18917-3_27.
- MacLeod, K.G., 1994. Extinction of inoceramid bivalves in Maastrichtian strata of the Bay of Biscay region of France and Spain. *Journal of Paleontology* 68, 1048–1066. <https://doi.org/10.1017/S0022336000026652>.
- MacLeod, K.G., Huber, B.T., 1996. Strontium isotopic evidence for extensive reworking in sediments spanning the Cretaceous-Tertiary boundary at ODP Site 738. *Geology* 24, 463–466. [https://doi.org/10.1130/0091-7613\(1996\)024<0463:SIEFER>2.3.CO;2](https://doi.org/10.1130/0091-7613(1996)024<0463:SIEFER>2.3.CO;2).
- MacLeod, K.G., Huber, B.T., 2001. The Maastrichtian record at Blake Nose (western North Atlantic) and implications for global palaeoceanographic and biotic changes. *Geological Society, London, Special Publications* 183, 111–130. <https://doi.org/10.1144/GSL.SP.2001.183.01.06>.
- MacLeod, K.G., Huber, B.T., Ward, P.D., 1996. The biostratigraphy and paleobiogeography of Maastrichtian inoceramids. *Geological Society of America Special Paper* 307, 361–373.
- MacLeod, K.G., Isaza Londoño, C., Martin, E.E., Jiménez Berrocoso, Á., Basak, C., 2011. Changes in North Atlantic circulation at the end of the Cretaceous greenhouse interval. *Nature Geoscience* 4, 779–782. <https://doi.org/10.1038/ngeo1284>.
- MacLeod, K.G., Ward, P.D., 1990. Extinction pattern of Inoceramus (Bivalvia) based on shell fragment biostratigraphy. *Geological Society of America Special Paper* 247, 509–518.
- Martin, E.E., MacLeod, K.G., Jiménez Berrocoso, A., Bourbon, E., 2012. Water mass circulation on Demerara Rise during the Late Cretaceous based on Nd isotopes. *Earth and Planetary Science Letters* 327–328, 111–120. <https://doi.org/10.1016/j.epsl.2012.01.037>.
- Mayer, B., Boyer, E.W., Goodale, C., Jaworski, N.A., Van Breemen, N., Howarth, R.W., Seitzinger, S., Billen, G., Lajtha, K., Nadelhoffer, K., Van Dam, D., Hetling, L.J., Nosal, M., Paustian, K., 2002. Sources of nitrate in rivers draining sixteen watersheds in the northeastern U.S.: Isotopic constraints. *Biogeochemistry* 57, 171–197. <https://doi.org/10.1023/A:1015744002496>.
- Mayot, N., Le Quéré, C., Rödenbeck, C., Bernardello, R., Bopp, L., Djeutchouang, L.M., Gehlen, M., Gregor, L., Gruber, N., Hauck, J., Iida, Y., Ilyina, T., Keeling, R.F., Landschützer, P., Manning, A.C., Pataru, L., Resplandy, L., Schwinger, J., Séférian, R., Watson, A.J., Wright, R.M., Zeng, J., 2023. Climate-driven variability of the Southern Ocean CO₂ sink. *Philosophical Transactions of the Royal Society A* 381. <https://doi.org/10.1098/rsta.2022.0055> 20220055.
- McCorkle, D.C., Keigwin, L.D., Corliss, B.H., Emerson, S.R., 1990. The influence of microhabitats on the carbon isotopic composition of deep-sea benthic foraminifera. *Paleoceanography* 5, 161–185. <https://doi.org/10.1029/PA005i002p00161>.
- Miller, K.G., Barrera, E., Olsson, R.K., Sugarman, P.J., Savin, S.M., 1999. Does ice drive early Maastrichtian eustasy? *Geology* 27. [https://doi.org/10.1130/0091-7613\(1999\)027<0783:DIDEME>2.3.CO;2](https://doi.org/10.1130/0091-7613(1999)027<0783:DIDEME>2.3.CO;2) 783.
- Miller, K.G., Browning, J.V., Schmelz, W.J., Kopp, R.E., Mountain, G.S., Wright, J.D., 2020. Cenozoic sea-level and cryospheric evolution from deep-sea geochemical and continental margin records. *Science Advances* 6 (20). <https://doi.org/10.1126/sciadv.aaz1346>.
- Morris, N.J., 1995. Maastrichtian Inoceramidae from the United Arab Emirates-Oman border region. *Bulletin of the British Museum (Natural History). Geology Series* 51, 257–265.
- Müller, R.D., Gaina, C., Tikku, A., Mihut, D., Cande, S.C., Stock, J.M., 2000. Mesozoic/Cenozoic tectonic events around Australia. In: Richards, M.A., Gordon, R.G., Van Der Hilst, R.D. (Eds.), *Geophysical Monograph Series* C. 121. American Geophysical Union, Washington, D, pp. 161–188. <https://doi.org/10.1029/GM121p0161>.
- Müller, R.D., Sdrölias, M., Gaina, C., Roest, W.R., 2008a. Age, spreading rates, and spreading asymmetry of the world's ocean crust. *Geochemistry Geophysics Geosystems* 9, Q04006. <https://doi.org/10.1029/2007GC001743>.
- Müller, R.D., Sdrölias, M., Gaina, C., Steinberger, B., Heine, C., 2008b. Long-term sea-level fluctuations driven by ocean basin dynamics. *Science* 319, 1357–1362. <https://doi.org/10.1126/science.1151540>.
- Murphy, D.P., Thomas, D.J., 2013. The evolution of Late Cretaceous deep-ocean circulation in the Atlantic basins: Neodymium isotope evidence from South Atlantic drill sites for tectonic controls: Cretaceous Atlantic deep circulation. *Geochemistry, Geophysics, Geosystems* 14, 5323–5340. <https://doi.org/10.1002/2013GC004889>.
- Nederbragt, A.J., 1989. Maastrichtian Heterohelicidae (Planktonic Foraminifera) from the North West Atlantic. *Journal of Micropaleontology* 8, 183–206. <https://doi.org/10.1144/jm.8.2.183>.
- Nederbragt, A.J., 1992. Paleocology of late Maastrichtian Heterohelicidae (planktic foraminifera) from the Atlantic region. *Palaeogeography, Palaeoclimatology, Palaeoecology* 92, 361–374. [https://doi.org/10.1016/0031-0182\(92\)90091-I](https://doi.org/10.1016/0031-0182(92)90091-I).
- Nicol, D., 1964. An essay on size of marine pelecypods. *Journal of Paleontology* 38, 968–974.
- Nifuku, K., Kodama, K., Shigeta, Y., Naruse, H., 2009. Faunal turnover at the end of the Cretaceous in the North Pacific region: Implications from combined

- magnetostratigraphy and biostratigraphy of the Maastrichtian Senpohshi Formation in the eastern Hokkaido Island, northern Japan. *Palaeogeography, Palaeoclimatology, Palaeoecology* 271, 84–95. <https://doi.org/10.1016/j.palaeo.2008.09.012>.
- Nobre Silva, I.G., Weis, D., Scoates, J.S., Barling, J., 2013. The Ninetyeast Ridge and its Relation to the Kerguelen, Amsterdam and St. Paul Hotspots in the Indian Ocean. *Journal of Petrology* 54, 1177–1210. <https://doi.org/10.1093/petrology/egt009>.
- Nyong, E.I., 1984. Campanian to lower Maastrichtian paleobiogeography of the Eastern North Atlantic region. *Eclogae Geologicae Helvetiae* 77, 469–481.
- Olsson, R.K., 1988. Foraminiferal modeling of sea-level change in the Late Cretaceous of New Jersey. In: Olsson, R.K. (Eds.), *Sea-Level Changes: an integrated approach*. Society of Economic Paleontologists and Mineralogists Special Publications 42, 289–297.
- Paquay, F.S., Ravizza, G., 2012. Heterogeneous seawater 187Os/188Os during the Late Pleistocene glaciations. *Earth and Planetary Science Letters* 349–350, 126–138. <https://doi.org/10.1016/j.epsl.2012.06.051>.
- Paytan, A., Gray, E.T., Ma, Z., Erhardt, A., Faul, K., 2012. Application of sulphur isotopes for stratigraphic correlation. *Isotopes in Environmental and Health Studies* 48, 195–206. <https://doi.org/10.1080/10256016.2011.625423>.
- Pergament, M.A., 1967. Steps in the development of inoceramids in the light of absolute geochronology. *Paleontologicheskij Zhurnal* 1, 32–40.
- Peryt, D., 1980. Planktic Foraminifera Zonation of the Upper Cretaceous in the Middle Vistula River Valley, Poland. *Palaeontologia Polonica* 41, 3–101.
- Peryt, D., Dubicka, Z., Wierny, W., 2022. Planktonic foraminiferal biostratigraphy of the Upper Cretaceous of the Central European Basin. *Geosciences* 12, <https://doi.org/10.3390/geosciences12010022>.
- Peucker-Ehrenbrink, B., Blum, J.D., 1998. Re-Os isotope systematics and weathering of Precambrian crustal rocks: implications for the marine osmium isotope record. *Geochimica Et Cosmochimica Acta* 62, 3193–3203. [https://doi.org/10.1016/S0016-7037\(98\)00227-0](https://doi.org/10.1016/S0016-7037(98)00227-0).
- Peucker-Ehrenbrink, B., Ravizza, G., 2000. The marine osmium isotope record. *Terra Nova* 12, 205–219. <https://doi.org/10.1046/j.1365-3121.2000.00295.x>.
- Philip, J., Floquet, M., Platel, J.P., Bergerat, F., Sandulescu, M., Baraboshkin, E., Amon, E., Poisson, A., Guiraud, R., Vaslet, D., Le Nindre, Y., Ziegler, M., Bouzid, S., Guezou, J.C., Lepvrier, C., 2000. Early Campanian (83–80 Ma). In: Dercourt, J., Gaetani, M., Vrielynck, B., Barrier, E., Bijou-Duval, B., Brunet, M.F., Cadet, J.P., Crasquin, S., Sandulescu, M. (Eds.), *Atlas Peri-Tethys, Paleogeographical Maps: CCGM/CGMW Paris, Map 15*.
- Pin, C., Briot, D., Bassin, C., Poitras, F., 1994. Concomitant separation of strontium and samarium-neodymium for isotopic analysis in silicate samples, based on specific extraction chromatography. *Analytica Chimica Acta* 298, 209–217. [https://doi.org/10.1016/0003-2670\(94\)00274-6](https://doi.org/10.1016/0003-2670(94)00274-6).
- Pisarzowska, A., Rakociński, M., Marynowski, L., Szczerba, M., Thoby, M., Paszkowski, M., Perri, M.C., Spalletta, C., Schönlaub, H.-P., Kowalik, N., Gereke, M., 2020. Large environmental disturbances caused by magmatic activity during the Late Devonian Hangenberg Crisis. *Global and Planetary Change* 190, <https://doi.org/10.1016/j.gloplacha.2020.103155>.
- Požaryski, W., 1948. Jura i kreda między Radomiem, Zawichostem i Kraśnikiem. (Jurassic and Cretaceous between Radom, Zawichost and Kraśnik, Central Poland). *Institute of Geology Bulletin* 46, 5–106. [In Polish]
- Puceat, E., Lecuyer, C., Reisberg, L., 2005. Neodymium isotope evolution of NW Tethyan upper ocean waters throughout the Cretaceous. *Earth and Planetary Science Letters* 236, 705–720. <https://doi.org/10.1016/j.epsl.2005.03.015>.
- Racki, G., 2020a. Big 5 Mass Extinctions. In: Elias, S., Alderton, D. (Eds.), *Encyclopedia of Geology*. Academic Press, pp. 603–611.
- Racki, G., 2020b. A volcanic scenario for the Frasnian-Famennian major biotic crisis and other Late Devonian global changes: More answers than questions? *Global and Planetary Change* 189, <https://doi.org/10.1016/j.gloplacha.2020.103174>.
- Racki, G., Marynowski, L., Rakociński, M., 2018a. Anomalous Upper Devonian mercury enrichments: comparison of Inductively Coupled Plasma – Mass Spectrometry (ICP-MS) and Atomic Absorption Spectrometry (AAS) analytical data. *Geological Quarterly* 62, 487–495.
- Racki, G., Rakociński, M., Marynowski, L., Wignall, P.B., 2018b. Mercury enrichments and the Frasnian-Famennian biotic crisis: A volcanic trigger proved? *Geology* 46, 543–546. <https://doi.org/10.1130/G40233.1>.
- Rakociński, M., Pisarzowska, A., Corradini, C., Narkiewicz, K., Dubicka, Z., Abdiev, N., 2021. Mercury spikes as evidence of extended arc-volcanism around the Devonian-Carboniferous boundary in the South Tian Shan (southern Uzbekistan). *Scientific Reports* 11, <https://doi.org/10.1038/s41598-021-85043-6>.
- Rakociński, M., Książak, D., Pisarzowska, A., Marynowski, L., 2022. Mercury evidence of intense submarine volcanism and hydrothermal activity during a mid-Tournaian anoxic event in the Carnic Alps. *Gondwana Research* 109, 225–238. <https://doi.org/10.1016/j.gr.2022.05.004>.
- Rakociński, M., Książak, D., Pisarzowska, A., Zatoń, M., Aretz, M., 2023. Weak and intermittent anoxia during the mid-Tournaian (Mississippian) anoxic event in the Montagne Noire, France. *Geological Magazine* 160, 831–854. <https://doi.org/10.1017/S0016756822001297>.
- Ravizza, G., 2007. Reconstructing the marine 187Os/188Os record and the particulate flux of meteoritic osmium during the late Cretaceous. *Geochimica Et Cosmochimica Acta* 71, 1355–1369. <https://doi.org/10.1016/j.gca.2006.11.006>.
- Ray, D.C., Van Buchem, F.S.P., Baines, G., Davies, A., Gréselle, B., Simmons, M.D., Robson, C., 2019. The magnitude and cause of short-term eustatic Cretaceous sea-level change: A synthesis. *Earth-Science Reviews* 197, <https://doi.org/10.1016/j.earscirev.2019.102901>.
- Rebotim, A., Voelker, A.H.L., Jonkers, L., Waniek, J.J., Meggers, H., Schiebel, R., Fraile, I., Schulz, M., Kucera, M., 2017. Factors controlling the depth habitat of planktonic foraminifera in the subtropical eastern North Atlantic. *Biogeosciences* 14, 827–859. <https://doi.org/10.5194/bg-14-827-2017>.
- Reusch, D.N., Ravizza, G., Maasch, K.A., Wright, J.D., 1998. Miocene seawater 187Os/188Os ratios inferred from metalliferous carbonates. *Earth and Planetary Science Letters* 160, 163–178. [https://doi.org/10.1016/S0012-821X\(98\)00082-X](https://doi.org/10.1016/S0012-821X(98)00082-X).
- Robaszynski, F., Bless, M.J.M., Felder, P.J., Foucher, J.C., Legoux, O., Manivit, H., Meesen, J.P.M.T., van der Tuuk, L.A., 1985. The Campanian-Maastrichtian boundary in the chalk facies close to the type-Maastricht area. *Bulletin Des Centres De Recherches Exploration-Production, Elf-Aquitaine* 9, 1–113.
- Rongemaille, E., Bayon, G., Pierre, C., Bollinger, C., Chu, N.C., Fouquet, Y., Riboulot, V., Voisset, M., 2011. Rare earth elements in cold seep carbonates from the Niger delta. *Chemical Geology* 286, 196–206. <https://doi.org/10.1016/j.chemgeo.2011.05.001>.
- Salazar-Jaramillo, S., Fowell, S.J., McCarthy, P.J., Benowitz, J.A., Śliwiński, M.G., Tomsich, C.S., 2016. Terrestrial isotopic evidence for a Middle-Maastrichtian warming event from the lower Cantwell Formation, Alaska. *Palaeogeography, Palaeoclimatology, Palaeoecology* 441, 360–376.
- Sames, B., Wagreich, M., Conrad, C.P., Iqbal, S., 2020. Aquifer-eustasy as the main driver of short-term sea-level fluctuations during Cretaceous hothouse climate phases. *Geological Society, London, Special Publications* 498, 9–38. <https://doi.org/10.1144/SP498-2019-105>.
- Sanei, H., Grasby, S.E., Beauchamp, B., 2012. Latest Permian mercury anomalies. *Geology* 40, 63–66. <https://doi.org/10.1130/G32596.1>.
- Schmittner, A., Bostock, H.C., Cartapanis, O., Curry, W.B., Filippson, H.L., Galbraith, E. D., Gottschalk, J., Herguera, J.C., Hoogakker, B., Jaccard, S.L., Lisiecki, L.E., Lund, D. C., Martínez-Méndez, G., Lynch-Stieglitz, J., Mackensen, A., Michel, E., Mix, A.C., Oppo, D.W., Peterson, C.D., Repschläger, J., Sikes, E.L., Spero, H.J., Waelbroeck, C., 2017. Calibration of the carbon isotope composition ($\delta^{13}C$) of benthic foraminifera. *Paleoceanography* 32, 512–530. <https://doi.org/10.1002/2016PA003072>.
- Shen, J., Algeo, T.J., Chen, J., Planavsky, N.J., Feng, Q., Yu, J., Liu, J., 2019. Mercury in marine Ordovician/Silurian boundary sections of South China is sulfide-hosted and non-volcanic in origin. *Earth and Planetary Science Letters* 511, 130–140. <https://doi.org/10.1016/j.epsl.2019.01.028>.
- Sial, A.N., Chen, J., Lacerda, L.D., Frei, R., Tewari, V.C., Pandit, M.K., Gaucher, C., Ferreira, V.P., Cirilli, S., Peralta, S., Korte, C., Barbosa, J.A., Pereira, N.S., 2016. Mercury enrichment and Hg isotopes in Cretaceous-Paleogene boundary successions: Links to volcanism and palaeoenvironmental impacts. *Cretaceous Research* 66, 60–81. <https://doi.org/10.1016/j.cretres.2016.05.006>.
- Sial, A.N., Gaucher, C., Filho, M.A. da S., Ferreira, V.P., Pimentel, M.M., Lacerda, L.D., Filho, E.V.S., Cezario, W., 2010. C-, Sr-isotope and Hg chemostratigraphy of Neoproterozoic cap carbonates of the Sergipano Belt, Northeastern Brazil. *Precambrian Research* 182, 351–372. <https://doi.org/10.1016/j.precamres.2010.05.008>.
- Sikes, C.S., Okazaki, K., Fink, R.D., 1981. Respiratory CO₂ and the supply of inorganic carbon for calcification of sea urchin embryos. *Comparative Biochemistry and Physiology Part a: Physiology* 70, 285–291. [https://doi.org/10.1016/0300-9629\(81\)90181-X](https://doi.org/10.1016/0300-9629(81)90181-X).
- Skelton, P.W. (Ed.), 2003. *The Cretaceous World*, Cambridge University Press, Cambridge.
- Soudry, D., Glenn, C.R., Nathan, Y., Segal, I., VonderHaar, D., 2006. Evolution of Tethyan phosphogenesis along the northern edges of the Arabian-African shield during the Cretaceous-Eocene as deduced from temporal variations of Ca and Nd isotopes and rates of P accumulation. *Earth-Science Reviews* 78, 27–57. <https://doi.org/10.1016/j.earscirev.2006.03.005>.
- Soudry, D., Glenn, C.R., Nathan, Y., Segal, I., VonderHaar, D., 2006. Evolution of Tethyan phosphogenesis along the northern edges of the Arabian-African shield during the Cretaceous-Eocene as deduced from temporal variations of Ca and Nd isotopes and rates of P accumulation. *Earth-Science Reviews* 78, 27–57. <https://doi.org/10.1016/j.earscirev.2006.03.005>.
- Speden, I.G., 1970. Generic status of the *Inoceramus?* *Tegulatus* species group (Bivalvia) of the latest Cretaceous of North America and Europe. *Postilla* 145, 1–45.
- Spero, H.J., Bijma, J., Lea, D.W., Bemis, B.E., 1997. Effect of seawater carbonate concentration on foraminiferal carbon and oxygen isotopes. *Nature* 390, 497–500. <https://doi.org/10.1038/37333>.
- Środoń, J., Drits, V.A., McCarty, D.K., Hsieh, J.C.C., Eberl, D.D., 2001. Quantitative XRD analysis of clay-rich rocks from random preparations. *Clays and Clay Minerals* 49, 514–528. <https://doi.org/10.1346/CCMN.2001.0490604>.
- Stanley, S.M., 1987. *Extinction*. Scientific American Library series. Scientific American Library. Distributed by W.H. Freeman, New York.
- Stemmerik, L., Surlyk, F., Klitten, K., Rasmussen, S.L., Schovsbo, N., 2006. Shallow core drilling of the Upper Cretaceous Chalk at Stevns Klint, Denmark. *Geological Survey of Denmark and Greenland Bulletin* 10, 13–16. <https://doi.org/10.34194/geusb.v10.4880>.
- Stille, P., Steinmann, M., Riggs, S.R., 1996. Nd isotope evidence for the evolution of the paleooccurants in the Atlantic and Tethys Oceans during the past 180 Ma. *Earth and Planetary Science Letters* 144, 9–19. [https://doi.org/10.1016/0012-821X\(96\)00157-4](https://doi.org/10.1016/0012-821X(96)00157-4).
- Surlyk, F., Bjerager, M., Damholt, T., 2006. Stevns Klint, Denmark: Uppermost Maastrichtian chalk, Cretaceous-Tertiary boundary, and lower Danian bryozoan mound complex. *Bulletin of the Geological Society of Denmark* 54, 1–48. <https://doi.org/10.37570/bgsd-2006-54-01>.
- Surlyk, F., Rasmussen, S.L., Boussaha, M., Schiøler, P., Schovsbo, N.H., Sheldon, E., Stemmerik, L., Thibault, N., 2013. Upper Campanian-Maastrichtian

- holostratigraphy of the eastern Danish Basin. *Cretaceous Research* 46, 232–256. <https://doi.org/10.1016/j.cretres.2013.08.006>.
- Swinburne, N.H.M., 1991. Tethyan extinctions, sea-level changes and the Sr-isotope curve in the 10 Ma. Preceding the K/T boundary. *Eos [transactions, American Geophysical Union]* 72, 267.
- Tachikawa, K., Arsouze, T., Bayon, G., Bory, A., Colin, C., Dutay, J.-C., Frank, N., Giraud, X., Gourlan, A.T., Jeandel, C., Lacan, F., Meynadier, L., Montagna, P., Piotrowski, A. M., Plancherel, Y., Pucéat, E., Roy-Barman, M., Waelbroeck, C., 2017. The large-scale evolution of neodymium isotopic composition in the global modern and Holocene ocean revealed from seawater and archive data. *Chemical Geology* 457, 131–148. <https://doi.org/10.1016/j.chemgeo.2017.03.018>.
- Tapia, R., Ho, S.L., Wang, H.-Y., Groeneveld, J., Mohtadi, M., 2022. Contrasting vertical distributions of recent planktic foraminifera off Indonesia during the southeast monsoon: implications for paleoceanographic reconstructions. *Biogeosciences* 19, 3185–3208. <https://doi.org/10.5194/bg-19-3185-2022>.
- Theiling, B.P., Coleman, M., 2015. Refining the extraction methodology of carbonate associated sulfate: Evidence from synthetic and natural carbonate samples. *Chemical Geology* 411, 36–48. <https://doi.org/10.1016/j.chemgeo.2015.06.018>.
- Thibault, N., Gardin, S., Galbrun, B., 2010. Latitudinal migration of calcareous nannofossil *Miculamurus* in the Maastrichtian: Implications for global climate change. *Geology* 38, 203–206. <https://doi.org/10.1130/G30326.1>.
- Thibault, N., Harlou, R., Schovsbo, N., Schiøler, P., Minoletti, F., Galbrun, B., Lauridsen, B.W., Sheldon, E., Stemmerik, L., Surlyk, F., 2012. Upper Campanian-Maastrichtian nannofossil biostratigraphy and high-resolution carbon-isotope stratigraphy of the Danish Basin: towards a standard $\delta^{13}C$ curve for the Boreal Realm. *Cretaceous Research* 33, 72–90. <https://doi.org/10.1016/j.cretres.2011.09.001>.
- Thibault, N., Husson, D., Harlou, R., Gardin, S., Galbrun, B., Huret, E., Minoletti, F., 2012. Astronomical calibration of upper Campanian-Maastrichtian carbon isotope events and calcareous plankton biostratigraphy in the Indian Ocean (ODP Hole 762C): implication for the age of the Campanian-Maastrichtian boundary. *Palaeogeography, Palaeoclimatology, Palaeoecology* 337–338, 52–71. <https://doi.org/10.1016/j.palaeo.2012.03.027>.
- Thibault, N., Husson, D., 2016. Climatic fluctuations and sea-surface water circulation patterns at the end of the Cretaceous era: Calcareous nannofossil evidence. *Palaeogeography, Palaeoclimatology, Palaeoecology* 441, 152–164. <https://doi.org/10.1016/j.palaeo.2015.07.049>.
- Thibault, N., Anderskov, K., Bjerager, M., Boldreel, L.O., Jelby, M.E., Stemmerik, L., Surlyk, F., 2015. Upper Campanian-Maastrichtian chronostratigraphy of the Skælskør-1 core, Denmark: correlation at the basinal and global scale and implications for changes in sea-surface temperatures. *Lethaia* 48, 549–560. <https://doi.org/10.1111/let.12128>.
- Thibault, N., Harlou, R., Schovsbo, N.H., Stemmerik, L., Surlyk, F., 2016. Late Cretaceous (late Campanian–Maastrichtian) sea-surface temperature record of the Boreal Chalk Sea. *Climate of the past* 12, 429–438. <https://doi.org/10.5194/cp-12-429-2016>.
- Tröger, K.-A., 1976. Evolutionary trends of Upper Cretaceous inoceramids. *Evolutionary Biology*, Praha, 193–203.
- Tröger, K.-A., Röhlich, P., 1991. Campanian-Maastrichtian inoceramid (*Bivalvia*) assemblages from NW Libya. In: Salem, O.S. (Ed.), *The Geology of Libya*, 4. Elsevier, Amsterdam, pp. 1357–1382.
- Ullmann, C.V., Korte, C., 2015. Diagenetic alteration in low-Mg calcite from macrofossils: a review. *Geological Quarterly* 59, 3–20. <https://doi.org/10.7306/gq.1217>.
- Van Der Zwaan, G.J., Duijnste, I.A.P., Den Dulk, M., Ernst, S.R., Jannink, N.T., Kouwenhoven, T.J., 1999. Benthic foraminifers: proxies or problems? *Earth-Science Reviews* 46, 213–236. [https://doi.org/10.1016/S0012-8252\(99\)00011-2](https://doi.org/10.1016/S0012-8252(99)00011-2).
- Vancoppenolle, I., Vellekoop, J., Doubrava, M., Kaskes, P., Sinnesael, M., Jagt, J.W.M., Claeys, P., Speijer, R.P., 2022. The benthic foraminiferal response to the mid-Maastrichtian event in the NW-European chalk sea of the Maastrichtian type area. *Netherlands Journal of Geosciences* 101, e12.
- Veron, J.E.N., 2011. Mass Extinctions, Anoxic Events and Ocean Acidification. In: Hopley, D. (Ed.), *Encyclopedia of Modern Coral Reefs*, Encyclopedia of Earth Sciences Series. Springer, Netherlands, Dordrecht, pp. 671–678. https://doi.org/10.1007/978-90-481-2639-2_37.
- Voigt, S., 1995. Palaeobiogeography of early Late Cretaceous inoceramids in the context of a new global palaeogeography. *Cretaceous Research* 16, 343–356. <https://doi.org/10.1006/cres.1995.1025>.
- Voigt, S., Friedrich, O., Norris, R.D., Schönfeld, J., 2010. Campanian – Maastrichtian carbon isotope stratigraphy: shelf-ocean correlation between the European shelf sea and the tropical Pacific Ocean. *Newsletter on Stratigraphy* 44, 57–72.
- Voigt, S., Gale, A.S., Jung, C., Jenkyns, H.C., 2012. Global correlation of Upper Campanian – Maastrichtian successions using carbon-isotope stratigraphy: development of a new Maastrichtian timescale. *Newsletters on Stratigraphy* 45, 25–53. <https://doi.org/10.1127/0078-0421/2012/0016>.
- Voigt, S., Jung, C., Friedrich, O., Frank, M., Teschner, C., Hoffmann, J., 2013. Tectonically restricted deep-ocean circulation at the end of the Cretaceous greenhouse. *Earth and Planetary Science Letters* 369–370, 169–177. <https://doi.org/10.1016/j.epsl.2013.03.019>.
- Voss, M., Deutsch, B., Elmgren, R., Humborg, C., Kuuppo, P., Pastuszak, M., Rolff, C., Schulte, U., 2006. Source identification of nitrate by means of isotopic tracers in the Baltic Sea catchments. *Biogeosciences* 3, 663–676. <https://doi.org/10.5194/bg-3-663-2006>.
- Walaszczyk, I., 2004. Inoceramids and inoceramid biostratigraphy of the Upper Campanian to basal Maastrichtian of the Middle Vistula River section, central Poland. *Acta Geologica Polonica* 54, 95–168.
- Walaszczyk, I., 2012. Integrated stratigraphy of the Campanian-Maastrichtian boundary succession of the Middle Vistula River (central Poland) section; introduction. *Acta Geologica Polonica* 62, 485–493.
- Walaszczyk, I., Jagt, J.W.M., Keutgen, N., 2010. The youngest Maastrichtian 'true' inoceramids from the Vijlen Member (Gulpen Formation) in northeast Belgium and the Aachen area (Germany). *Netherlands Journal of Geosciences* 89, 147–167. <https://doi.org/10.1017/S0016774600000755>.
- Walaszczyk, I., Kennedy, W.J., 2011. The inoceramid fauna and inoceramid-based correlations of the Calcaire a Baculites (Maastrichtian) of the Cotentin Peninsula, Manche, France. *Freiberger Forschungshefte C540*, 103–118.
- Walaszczyk, I., Kennedy, W.J., Klinger, H.C., 2009. Cretaceous faunas from Zululand and Natal, South Africa. Systematic palaeontology and stratigraphical potential of the Upper Campanian-Maastrichtian Inoceramidae (*Bivalvia*). *African Natural History* 5, 49–132.
- Watkins, D.K., Self-Trail, J.M., 2005. Calcareous nannofossil evidence for the existence of the Gulf Stream during the late Maastrichtian. *Paleoceanography* 20, 2004PA001121. [10.1029/2004PA001121](https://doi.org/10.1029/2004PA001121).
- Wedepohl, K.H., 1991. The composition of the upper earth's crust and the natural cycles of selected metals. Metals in natural raw materials. *Natural Resources*. In: Merian, E. (Ed.), *Metals and Their Compounds in the Environment*. Weinheim, Verlag Chemie (VCH), pp. 3–17.
- Weis, D., Frey, F.A., 1991. Isotope geochemistry of Ninetyeast Ridge basement basalts: Sr, Nd, and Pb evidence for involvement of the Kerguelen hot spot. In: Weissel, J., Peirce, J., Taylor, E., Alt, J. et al. (Eds), *Proceedings of the Ocean Drilling Program, Scientific Results*, 121. College Station, TX: Ocean Drilling Program 591–610.
- Wendler, I., Huber, B.T., MacLeod, K.G., Wendler, J.E., 2013. Stable oxygen and carbon isotope systematics of exquisitely preserved Turonian foraminifera from Tanzania – Understanding isotopic signatures in fossils. *Marine Micropaleontology* 102, 1–33. <https://doi.org/10.1016/j.marmicro.2013.04.003>.
- Westerhold, T., Marwan, N., Drury, A.J., Liebrand, D., Agnini, C., Anagnostou, E., Barnett, J.S.K., Bohaty, S.M., De Vleeschouwer, D., Florindo, F., Frederichs, T., Hodell, D.A., Holbourn, A.E., Kroon, D., Lauretano, V., Littler, K., Lourens, L.J., Lyle, M., Pälike, H., Röhl, U., Tian, J., Wilkens, R.H., Wilson, P.A., Zachos, J.C., 2020. An astronomically dated record of Earth's climate and its predictability over the last 66 million years. *Science* 369, 1383–1387. <https://doi.org/10.1126/science.aba6853>.
- Wetzel, A., 1987. Ichnofabrics in Eocene to Maastrichtian sediments from Deep Sea Drilling Project Site 605, off the New Jersey coast. *Deep Sea Drilling Project. Initial Reports* 92, 825–835.
- Wiese, F., Zobel, K., Keupp, H., 2015. Calcareous dinoflagellate cysts and the Turonian nutrient crisis – Data from the upper Turonian of the Lower Saxony Basin (northern Germany). *Cretaceous Research* 56, 673–688. <https://doi.org/10.1016/j.cretres.2015.06.007>.
- Wiese, F., Zobel, K., Mortimore, R.N., 2018. Intrinsic processes control late Turonian calcareous dinoflagellate cyst assemblages – A case study from the Sussex chalk (England). *Cretaceous Research* 87, 206–217. <https://doi.org/10.1016/j.cretres.2017.04.003>.
- Woodhead, J., Brauns, M., 2004. Current limitations to the understanding of Re–Os behaviour in subduction systems, with an example from New Britain. *Earth and Planetary Science Letters* 221, 309–323. [https://doi.org/10.1016/S0012-821X\(04\)00091-3](https://doi.org/10.1016/S0012-821X(04)00091-3).
- Ziegler, P.A., 1990. *Geological Atlas of Western and Central Europe*. Geological Society Publishing House, Bath, Shell Internationale Petroleum Maatschappij B. V.